THE JOURNAL OF BIOLOGICAL CHEMISTRY VOL. 287, NO. 42, pp. 35260–35274, October 12, 2012
Published in the U.S.A.

Structure/Function Relationships of Adipose Phospholipase A_2 Containing a Cys-His-His Catalytic Triad*[S]

Received for publication, July 6, 2012, and in revised form, August 8, 2012 Published, JBC Papers in Press, August 25, 2012, DOI 10.1074/jbc.M112.398859

Xiao-Yan Pang[‡1], Jian Cao[§1], Linsee Addington[‡], Scott Lovell[¶], Kevin P. Battaile[‖], Na Zhang[¶], J. L. Uma Maheswar Rao[‡], Edward A. Dennis[§], and Alexander R. Moise[‡2]

From the [‡]Department of Pharmacology and Toxicology, School of Pharmacy, University of Kansas, Lawrence, Kansas 66045, [§]Departments of Chemistry and Biochemistry and Pharmacology, School of Medicine, University of California San Diego, La Jolla, California 92093, [¶]Del Shankel Structural Biology Center, University of Kansas, Lawrence, Kansas 66047, and [‖]Industrial Macromolecular Crystallography Association Collaborative Access Team (IMCA-CAT), Hauptman-Woodward Medical Research Institute, Argonne, Illinois 60439

Background: AdPLA is the predominant phospholipase in adipose tissue where it suppresses lipolysis.
Results: AdPLA associates with membranes and displays PLA_2 and PLA_1 activities using a Cys-His-His catalytic triad.
Conclusion: The enzymatic mechanism and structure of AdPLA resembles that of NlpC/P60 cysteine peptidases.
Significance: The structure and enzymatic properties of AdPLA shed light on its physiological function.

Adipose phospholipase A_2 (AdPLA or Group XVI PLA_2) plays an important role in the onset of obesity by suppressing adipose tissue lipolysis. As a consequence, AdPLA-deficient mice are resistant to obesity induced by a high fat diet or leptin deficiency. It has been proposed that AdPLA mediates its antilipolytic effects by catalyzing the release of arachidonic acid. Based on sequence homology, AdPLA is part of a small family of acyltransferases and phospholipases related to lecithin:retinol acyltransferase (LRAT). To better understand the enzymatic mechanism of AdPLA and LRAT-related proteins, we solved the crystal structure of AdPLA. Our model indicates that AdPLA bears structural similarity to proteins from the NlpC/P60 family of cysteine proteases, having its secondary structure elements configured in a circular permutation of the classic papain fold. Using both structural and biochemical evidence, we demonstrate that the enzymatic activity of AdPLA is mediated by a distinctive Cys-His-His catalytic triad and that the C-terminal transmembrane domain of AdPLA is required for the interfacial catalysis. Analysis of the enzymatic activity of AdPLA toward synthetic and natural substrates indicates that AdPLA displays PLA_1 in addition to PLA_2 activity. Thus, our results provide insight into the enzymatic mechanism and biochemical properties of AdPLA and LRAT-related proteins and lead us to propose an alternate mechanism for AdPLA in promoting adipose tissue lipolysis that is not contingent on the release of arachidonic acid and that is compatible with its combined PLA_1/A_2 activity.

Adipose tissue plays an important role in the regulation of energy balance. Although most other tissues can hydrolyze triacylglycerols for their own use, adipose tissue alone can hydrolyze triacylglycerols to export glycerol and fatty acids for use by other tissues. The net rate of triacylglycerol hydrolysis in adipose tissue (or lipolysis) is a determinant of whole-body insulin sensitivity (1) and hence a potentially important therapeutic target in the treatment of obesity. Adipose tissue lipolysis proceeds through the sequential action of the triacylglycerol hydrolases, desnutrin/adipose triglyceride lipase (2–4), hormone-sensitive lipase (5, 6), and monoglyceride lipase (7). The rate of adipose tissue lipolysis is carefully controlled by endocrine mediators, such as insulin and catecholamines, and locally through the action of autocrine/paracrine signaling mediators (8).

In addition to defining the structure and permeability of cells and cellular organelles, phospholipids are a source of locally acting signaling mediators. Hydrolysis of fatty acids linked to the *sn*-1 or *sn*-2 positions of phospholipids by phospholipase A_1 (PLA_1)[3] or A_2 (PLA_2) enzymes, respectively, leads to formation of lipid signaling mediators, such as free fatty acids and lysophospholipids (for a review, see Ref. 9). Adipose phospholipase A_2 (AdPLA) classified as Group XVI PLA_2 (PLA2G16) (9) is the most abundant PLA_2 in adipose tissue (10, 11), and its expression increases during adipose differentiation (12). Expression of AdPLA is also up-regulated by feeding and by insulin *in vivo* (11). Importantly, AdPLA was shown to control adipose tissue lipolysis via the production of eicosanoid mediators (11). The level of the prostaglandin PGE_2 was shown to be markedly reduced in the adipose tissue of *AdPLA*−/− mice (11). PGE_2

* This work was supported, in whole or in part, by National Institutes of Health Grants 5P20RR017708-10 and 3P20RR017708-07S1, subawards of grants from the National Center for Research Resources (to A. R. M.), Grant 8 P20 GM103420-10) from the NIGMS (to A. R. M.), and Grant R01 GM20501 (to E. A. D.).

[S] This article contains supplemental Figs. S1–S4.

The atomic coordinates and structure factors (code 4FA0) have been deposited in the Protein Data Bank, Research Collaboratory for Structural Bioinformatics, Rutgers University, New Brunswick, NJ (http://www.rcsb.org/).

[1] Both authors contributed equally to this work.

[2] To whom correspondence should be addressed: Dept. of Pharmacology and Toxicology, School of Pharmacy, 5060-Malott Hall, 1251 Wescoe Hall Dr., University of Kansas, Lawrence, KS 66045. Tel.: 785-864-1010; E-mail: alexmoise@ku.edu.

[3] The abbreviations used are: PLA, phospholipase A; AdPLA, adipose phospholipase A_2; LRAT, lecithin:retinol acyltransferase; PGE_2, prostaglandin E_2; DXMS, hydrogen/deuterium exchange experiments coupled to mass spectrometry; T-AdPLA, truncation of human AdPLA; MBP, maltose-binding protein; TEV, tobacco etch virus; FL-AdPLA, full-length AdPLA; PC, phosphatidylcholine; PG, phosphatidylglycerol; BODIPY, boron-dipyrromethene; BODIPY PC-A2, 1-*O*-(6-BODIPY 558/568-aminohexyl)-2-BODIPY FL C5-*sn*-glycero-3-phosphocholine; BODIPY FL C5, 3a,4a-diaza-*s*-indacene-3-pentanoic acid; LPA, lysophosphatidic acid; CGI-58, comparative gene identification-58.

activates prostaglandin E receptor 3, which suppresses lipolysis in a cAMP-dependent manner (13). As a result, *AdPLA*−/− mice have increased rates of lipolysis and fatty acid oxidation and higher energy expenditure than wild type mice (11). *AdPLA*−/− mice are lean and resistant to diet-induced obesity (11). Moreover, crossing *AdPLA*−/− mice with leptin-deficient (*ob*/*ob*) mice generates *AdPLA*−/−,*ob*/*ob* double knockout mice that gain considerably less weight than single knockout *ob*/*ob* leptin-deficient mice (11). These data suggest that AdPLA is an important regulator of the rate of adipose tissue lipolysis via production of prostanoid mediators.

The enzymatic activity of AdPLA was initially described to be a calcium-dependent PLA_2 utilizing a His-Cys catalytic dyad (10). Later reports described AdPLA to be a calcium-independent phospholipase with combined PLA_1, PLA_2, and transacylase activities; its PLA_1 activity was reported to be higher than its PLA_2 activity (14). The sequence and enzymatic activity of AdPLA resemble those of a small family of proteins related to lecithin:retinol acyltransferase (LRAT). All members of the LRAT family have been shown to catalyze PLA_1, PLA_2, or acyltransferase reactions (15–18). Thus, the LRAT family could be appropriately described as a phospholipase A/acyltransferase family based on a recent proposal by Uyama *et al.* (19). In this case, AdPLA would be referred to as phospholipase A/acyltransferase-3.

The inhibitory effect of AdPLA expression on adipose tissue lipolysis was proposed to be a result of the production of PGE_2 through the release of arachidonic acid from the *sn*-2 position of phospholipids (11). However, the significant PLA_1 activity of AdPLA led to suggestions that AdPLA might have other functions in controlling cellular metabolism and lipid accumulation in addition to production of free arachidonic acid (14, 20). In one such example, overexpression of AdPLA in human embryonic kidney 293 (HEK293) cells (21) leads to peroxisome dysfunction and a decrease in ether-linked triglycerides and plasmalogens (22). Importantly, these effects were not accompanied by a significant release of arachidonic acid in such cells.

AdPLA was originally identified as being specifically expressed in phenotypic revertants of H-*ras*-transformed cells; thus, it was characterized as a class II tumor suppressor (23) and referred to as H-*ras*-revertant gene 107 (H-Rev107) or H-Ras-like suppressor 3 (HRASLS3). Expression of AdPLA is downregulated in several tumor cell lines (24–27); however, overexpression of AdPLA induces growth inhibition of transformed cells (28) and apoptosis of ovarian carcinoma cells (29). The relationship between the enzymatic activity and the tumor suppressive effect of AdPLA is not well understood.

To gain a better understanding of the physiological role of AdPLA, we investigated its structure and enzymatic properties. Based on sequence analysis, members of the LRAT family were predicted to have a circular permutation of the catalytic domain found in members of the superfamily of proteins related to *Escherichia coli* NlpC and *Listeria monocytogenes* P60 proteins (NlpC/P60) (30, 31). Several of the NlpC/P60 enzymes were suggested to utilize a conserved Cys-His pair or a Cys-His-His triad in their catalytic mechanism (32, 33). In the case of LRAT and other LRAT family members, the Cys residue was shown to act as a nucleophile and form a covalent thiol-acyl intermediate in the catalytic process (20, 34). A truncated fragment of AdPLA lacking the transmembrane domain was recently characterized by a solution NMR structure (35) and x-ray crystallography (20). Both structures show that AdPLA conforms to the permuted papain domain fold seen in a subset of NlpC/P60 proteins and predict the location of residues potentially involved in the catalytic triad of AdPLA.

Herein, we further describe the enzymatic mechanism of AdPLA by presenting a novel crystal structure of AdPLA that provides additional support for its enzymatic mechanism. We describe the expression and purification of a soluble full-length form of AdPLA that displays robust enzymatic activity, and we examine the PLA_1/PLA_2 specificity of AdPLA for various natural phospholipid substrates. We provide experimental support for the role of the residues proposed to be involved in the catalytic mechanism, and we probe the structural dynamic difference between full-length and truncated AdPLA based on hydrogen/deuterium exchange experiments coupled to mass spectrometry (DXMS). Finally, we evaluate the possible role of AdPLA in the generation of arachidonic acid in adipose tissue in light of its activity and substrate preference.

EXPERIMENTAL PROCEDURES

Cloning, Mutagenesis, and Purification of Full-length and Truncated AdPLA—We cloned human *AdPLA* cDNA from a full-length expressed sequence tag clone available from the Open Biosystems Mammalian Gene Collection (MGC) (MGC: 118754, IMAGE: 40000132). A truncation of human AdPLA (T-AdPLA) retaining amino acid residues 1–134 was amplified and cloned through ligation-independent cloning in the vector pTB-MalE (36) digested with SspI. The ligation places T-AdPLA downstream of an N-terminal fusion partner consisting of a hexahistidine-tagged maltose-binding protein (MBP) and a tobacco etch virus (TEV) protease cleavage site. Alternatively, the full-length AdPLA (FL-AdPLA) cDNA was cloned in-frame with MBP and separated by a TEV cleavage site to generate a construct coding for an MBP-FL-AdPLA fusion protein. Mutagenesis of the MBP-FL-AdPLA protein was performed using a QuikChange II XL site-directed mutagenesis kit (Stratagene, La Jolla, CA). The expression constructs were sequenced and transformed in Bl21(DE3) *E. coli* and grown in Terrific Broth under the selection of 100 μg/ml ampicillin and 25 μg/ml chloramphenicol. The primers used for cloning T-AdPLA and FL-AdPLA and for site-directed mutagenesis reactions of MBP-FL-AdPLA are shown in supplemental Fig. S1. The sequence of the expressed MBP-T-AdPLA and MBP-FL-AdPLA proteins are shown in supplemental Fig. S2.

Protein expression was induced using the Overnight Express Autoinduction System (EMD Millipore-Merck KGaA, Billerica, MA) based on a method described previously (37). The bacteria were harvested by centrifugation at 4,000 × *g* for 10 min at 4 °C. The pellet was resuspended in 50 mM Tris, pH 8.0, 500 mM NaCl, 5 mM β-mercaptoethanol, 10% glycerol, 25 units/ml Benzonase (EMD Millipore), 50 mM arginine and lysed either by two passages in a French press or through sonication at 50% amplitude for 6 × 20 s. The lysate was spun by centrifugation at 19,000 rpm for 30 min to pellet membranes and insoluble complexes and then filtered through a 0.2-μm filter.

Purification of MBP-FL-AdPLA or MBP-T-AdPLA fusion proteins was carried out by metal affinity chromatography. The bacterial supernatant was loaded onto tandem 5-ml His Trap HP columns (GE Healthcare) in conjunction with an ÄKTA Xpress purification system at a flow rate of 1 ml/min. The columns were washed with Buffer A (0.2% Triton X-100, 50 mM Tris, pH 8.0, 50 mM NaCl, 5 mM β-mercaptoethanol, 10% glycerol) over 4 column volumes. Another wash with 5% Buffer B (500 mM imidazole, 50 mM Tris, pH 8.0, 50 mM NaCl, 5 mM β-mercaptoethanol, 10% glycerol) was used to remove nonspecifically bound proteins. Elution was carried out with Buffer B in a linear gradient from 5 to 100%. The resulting fractions were examined by SDS-PAGE, and the protein-containing fractions were pooled and filtered through a 0.2-μm filter. The protein solution was concentrated and desalted using a Spin-X UF centrifugal concentrator (20 ml; 5,000 molecular weight cutoff; Corning Inc. Life Sciences, Tewksbury, MA) to a final concentration of 10 mg/ml in 50 mM Tris, pH 8.0, 50 mM NaCl, 5 mM β-mercaptoethanol. MBP-FL-AdPLA or MBP-T-AdPLA fusion proteins were next purified by anion exchange chromatography using tandem 5-ml HiTrap Q HP columns (GE Healthcare). The column was washed using Buffer A (50 mM Tris, pH 8.0, 50 mM NaCl) over 4 column volumes followed by a wash with 10% Buffer B (50 mM Tris, pH 8.0, 1.0 M NaCl, 5 mM β-mercaptoethanol) to remove nonspecifically bound proteins. Elution was carried out with Buffer B in a linear gradient from 10 to 100% at a flow rate of 1 ml/min, and the protein-containing fractions were pooled and filtered through a 0.2-μm filter. Cleavage with TEV to remove the MBP fusion was performed using 30 mg of MBP-T-AdPLA protein in 30 ml of 150 mM NaCl, 25 mM Tris, pH 8.0, 5 mM β-mercaptoethanol supplemented with 600 μg of hexahistidine-tagged TurboTEV (2 mg/ml stock; 10,000 units/mg; Nacalai USA, San Diego, CA) for 48 h at 20 °C with gentle shaking. The hexahistidine-tagged MBP and TurboTEV proteins were removed by metal affinity chromatography using 2 ml of HisPur nickel-nitrilotriacetic acid resin (Fisher Scientific) in sodium phosphate, pH 7.4, 10 mM imidazole, 5 mM β-mercaptoethanol. The eluted untagged T-AdPLA protein was filtered through a 0.2-μm filter and concentrated to 4 ml using a Spin-X UF centrifugal concentrator (20 ml; 5,000 molecular weight cutoff; Corning Inc. Life Sciences) and purified by using size exclusion chromatography on a HiLoad 16/600 Superdex 75 prep grade column equilibrated with a buffer of 50 mM Tris, pH 8.0, 300 mM NaCl, 5 mM dithiothreitol (DTT) and eluted at 0.8 ml/min over 2.5 column volumes. The T-AdPLA-containing fractions were pooled, filtered through a 0.2-μm filter, and concentrated to 10 mg/ml. The resulting untagged T-AdPLA protein is stable at 4 °C for more than 4 weeks. To verify the identity of the purified protein, the recombinant T-AdPLA protein was examined by SDS-PAGE. The purified protein migrated as a single band as identified by Coomassie Blue staining. The protein band was cut from the gel and treated with iodoacetamide to amidate the Cys residues and digested in-gel with L-1-tosylamido-2-phenylethyl chloromethyl ketone-treated trypsin. Analysis of the tryptic fragments by tandem MS/MS identified the purified protein as AdPLA showing 90% peptide coverage of the T-AdPLA protein (supplemental Fig. S3). The T-AdPLA protein was set up for crystallization screens or for enzyme assays.

In the case of FL-AdPLA, cleavage with TEV of the MBP-FL-AdPLA fusion protein results in precipitation of the FL-AdPLA protein; therefore, MBP-FL-AdPLA was purified sequentially by affinity chromatography, ion exchange chromatography, and size exclusion chromatography as described for MBP-T-AdPLA and then used as an intact MBP-FL-AdPLA fusion protein in enzyme assays. The uncleaved MBP-FL-AdPLA protein is stable at 4 °C for several months. We also expressed and purified a C-terminal truncated fragment of AdPLA representing the residues 1–132 of human AdPLA fused to an N-terminal hexahistidine tag denoted as His_6-AdPLA(1–132), which has been described previously (20). The plasmid coding for His_6-AdPLA(1–132) was obtained as a kind gift from Marcin Golczak and Kris Palczewski. The plasmid was used to express and purify the His_6-AdPLA(1–132) protein following the same procedure as that used for MBP-FL-AdPLA.

Crystallization, X-ray Diffraction, and Data Collection—A purified sample of T-AdPLA was screened for crystallization in Compact Jr. (Emerald Biosystems, Bainbridge Island, WA) sitting drop vapor diffusion plates at 20 °C using 0.5 μl of protein (10 mg/ml in 50 mM Tris, pH 8.0, 300 mM NaCl, 5 mM DTT) and 0.5 μl of crystallization solution equilibrated against 100 μl of the latter. Small prismatic crystals were obtained in 1–2 days from the Wizard 4 screen (Emerald Biosystems) condition 21 (25% polyethylene glycol (PEG) 1500, 100 mM malonate/imidazole/borate 2:3:3 (MIB) buffer, pH 5.0) and in ~1 week from the Wizard 3 screen condition 4 (Emerald Biosystems; 20% PEG 3350, 200 mM ammonium formate). Samples were transferred to a fresh drop composed of 80% crystallization solution and 20% PEG 200 before flash freezing in liquid nitrogen for data collection. Data were collected at the Advanced Photon Source beamline 17-ID using a Dectris Pilatus 6M pixel array detector.

Structure Solution and Refinement—Intensities were integrated using XDS (38), and the Laue class check and data scaling were performed with Aimless (39). The highest probability Laue class was $-3m1$ and space group $P3_121$ or $P3_221$. Matthews' coefficient (40) (V_m = 2.8/55.6%) indicated that there was a single AdPLA molecule in the asymmetric unit. Structure solution was conducted by molecular replacement with Phaser (41) via the PHENIX (42) interface. All space groups in the Laue class $-3m1$ were tested using a single molecule from a previously determined AdPLA NMR structure (Protein Data Bank code 2KYT) as the search model. The top solution was obtained in the space group $P3_121$ and was used from this point forward. Because of the anisotropy of the diffraction data, the model was refined with a resolution cutoff of 2.65 Å. Structure refinement and manual model building were conducted with BUSTER (43) and Coot (44), respectively. Structure validation was conducted with MolProbity (45). Figures were prepared using the CCP4MG package (46). The coordinates and structure factors were deposited in the Protein Data Bank under accession code 4FA0.

DXMS Experiments—Proteins were incubated in D_2O buffer consisting of 12 mM Tris, 50 mM NaCl in 99% D_2O, pD_{read} 7.5 as described previously (47). Exchange experiments were initiated by mixing 2 μg of T-AdPLA, MBP-T-AdPLA, or MBP-FL-AdPLA in protein buffer or with 6 μl of D_2O buffer to a final

concentration of 75% D_2O. The mixtures were incubated at 23 °C for 10, 30, 100, 300, 1,000, 3,000, or 10,000 s, and then the exchange reaction was quenched by adding 12 μl of ice-cold quench solution (0.96% formic acid, 0.8 M guanidine hydrochloride), resulting in samples with final concentrations of 0.58% formic acid and 0.5 M guanidine hydrochloride, pH 2.5. The samples were then immediately frozen on dry ice and stored at −80 °C.

Proteolysis-Liquid Chromatography-Mass Spectroscopy Analysis of Samples—All steps were performed at 0 °C as described previously (47). The digested peptides were separated by C_{18} column and detected using a Thermo Orbitrap Elite mass spectrometer. Data processing of DXMS experiments utilized specialized software as described previously (DXMS Explorer, Sierra Analytics Inc.) (47).

In Vitro Phospholipase Activity Assays—Liposomes were created using mixtures of phosphatidylcholine (PC) and phosphatidylglycerol (PG) phospholipids (Avanti Polar Lipids, Alabaster, AL). The PC species examined were 18:0-16:0 PC, 16:0-18:0 PC, 16:0-20:4 PC, 16:0-18:2 PC, 18:1-18:1 PC, 16:0 lyso-PC, and 18:0-18:0 diether PC. 100-μl aliquots from 10 mg/ml stock solutions of each of the PC species examined were mixed with an equal amount of 10 mg/ml 18:1-18:1 PG. The phospholipid mixture was dried down in a borosilicate glass test tube under vacuum to remove the solvent (chloroform). The lipid cake was hydrated in the presence of 50 mM Tris, pH 8, 100 mM NaCl, 1 mM $CaCl_2$ for 1 h at a temperature above the solid-fluid transition temperature (T_c) of the phospholipid mixture followed by sonication of the hydrated lipid for 10–30 min in a bath sonicator to produce a suspension of small unilamellar vesicles representing a concentration of 1 mM for the combined phospholipids in a ratio of 1:1 PC/PG. The assay was conducted by incubating purified MBP-FL-AdPLA, T-AdPLA, MBP-T-AdPLA, bee venom PLA_2 (Invitrogen), or *Thermomyces lanuginosus* lipase with *sn*-1,3 specificity (Lecitase Ultra-Novozymes A/S, Denmark; obtained from Invitrogen) for 15 min with various liposomes in the presence of 5 mM tris(2-carboxyethyl)-phosphine in a total volume of 220 μl. The reaction was stopped by adding 1 ml of Dole's reagent (48) (40 ml of isopropanol, 10 ml of heptane, and 1 ml of 1 M H_2SO_4) and vortexed for 5 min. The organic phase was extracted with 600 μl of heptane and 400 μl of water. Phase separation was induced by centrifugation at 3,000 rpm for 5 min; the organic phase was collected and dried down under vacuum. The residue was resuspended in 200 μl of a mixture of chloroform and methanol (1:1), 10 μl of which was injected into the HPLC system for analysis. Free fatty acids were analyzed by reverse-phase HPLC coupled to a charged aerosol detector using an HPLC1200 system (Agilent Technologies, Santa Clara, CA) equipped with a Halo C_8 column (150 × 4.6 mm; 2.7 μm; MAC-MOD Analytical, Inc., Chadds Ford, PA), mobile phase A composed of methanol/water/acetic acid (750:250:4), mobile phase B composed of acetonitrile/methanol/tetrahydrofuran/acetic acid (500:375:125:4), and a flow rate of 0.8 ml/min with a column temperature of 40 °C. The samples were injected in methanol/chloroform (1:1). The following gradient was used: 100% A to 30% A over 40 min, 30% A to 10% A over 20 min, and holding at 10% A for 5 min followed by re-equilibration in 100% A. The eluted lipids were detected using a Corona charged aerosol detector (ESA Biosciences) operated at 200 pA and 35-p.s.i. nitrogen pressure as described (49). Experimental samples consisting of various enzyme preparations or buffer control were set up in triplicate. Authentic fatty acid standards were used to establish the identity of the eluted peaks.

We also investigated the phospholipase activity of AdPLA using a boron-dipyrromethene (BODIPY)-labeled fluorogenic phospholipid substrate, 1-*O*-(6-BODIPY 558/568-aminohexyl)-2-BODIPY FL C5-*sn*-glycero-3-phosphocholine (BODIPY PC-A2; A10072, Invitrogen). Liposomes were prepared by the ethanolic injection method (50). Equal volumes of 10 mM 18:1-18:1 PC, 10 mM 18:1-18:1 PG, and 1 mM BODIPY PC-A2 were combined to prepare a lipid mixture containing 10:10:1 molar ratios of 18:1-18:1 PC/18:1-18:1 PG/BODIPY PC-A2. 10 μl of the lipid mixture was injected while vigorously vortexing in a glass tube containing 1 ml of buffer composed of 50 mm Tris, pH 8, 100 mM NaCl, 1 mM $CaCl_2$. 100 μl of liposome substrate was aliquoted in a 96-well plate and examined using a Synergy H1 multimode microplate reader equipped with dispensers (BioTek, Winooski, VT). The liposome suspension was allowed to equilibrate at 37 °C while the fluorescence signal at 488/515 nm was recorded for 1 min to monitor the background emission. No significant increase in background fluorescence emission was observed. Purified MBP-T-AdPLA, T-AdPLA, MBP-T-AdPLA, His_6-AdPLA(1–132), and wild type and mutants of MBP-FL-AdPLA were diluted in 50 mM Tris, pH 8, 100 mM NaCl, 1 mM $CaCl_2$; 100 μl of protein was dispensed in the well containing the liposome suspension; and the fluorescence signal at 488/515 nm was recorded for the next 4 min. To calculate the rate of reaction as a function of the amount of enzyme, we used a final concentration of BODIPY PC-A2 of 1.67 μM, whereas the protein concentration ranged from 7.8 to 125 μg/ml (0.12–1.9 μM). A standard curve of the fluorescence signal at 488/515 nm of 3a,4a-diaza-*s*-indacene-3-pentanoic acid (BODIPY FL C5; D3834, Invitrogen), the cleavage product of BODIPY PC-A2, was used for evaluating the percentage of substrate conversion. To measure enzyme velocities as a function of substrate concentration, we used a titration of substrate concentrations in molar excess of enzyme concentrations. Initial rates of reaction for various substrate concentrations were derived from steady-state kinetic measurements based on rates measured in the first 20 s of the reaction. The assay was carried out in triplicate, and the data were evaluated using the SigmaPlot and GraphPad software packages.

RESULTS

The Crystal Structure of AdPLA Reveals the Geometry of the Active Site—We tested several strategies to express human AdPLA as a recombinant protein in *E. coli* for structural studies. It was shown that the C-terminal domain of AdPLA is embedded in the membrane, whereas the N terminus of the AdPLA protein is found in the cytoplasm (10, 51). Analysis of the amino acid sequence of AdPLA reveals the absence of a cleavable signal sequence and the presence of a single hydrophobic domain at its C terminus. In accordance with this model, the C-terminal domain is required for targeting AdPLA to the membrane of the endoplasmic reticulum (10) by acting as a both a targeting signal and a membrane anchor domain (51). To increase the yield of soluble protein, we tested the effect of

removing the C-terminal hydrophobic domain and expressed both the full-length and the truncated version of AdPLA fusion proteins with a hexahistidine-tagged MBP protein to increase their solubility (52). The linker between the MBP and AdPLA contains a TEV cleavage site (ENLIF(Q/S)), allowing the MBP fusion partner to be cleaved with TEV protease and removed in the final stages of purification. Cleavage with TEV protease produces a protein that retains the sequence of either FL-AdPLA or T-AdPLA and a stretch of three additional amino acids (SNA-) at the N terminus of the recombinant proteins (supplemental Fig. S2).

Our results indicate that the presence of the C-terminal hydrophobic domain adversely affects the solubility of the bacterially expressed AdPLA protein. Although MBP-FL-AdPLA is a soluble protein, upon cleavage with TEV protease, the FL-AdPLA protein precipitated from solution. Inclusion of chaotropic agents and detergents led to only a modest improvement in the solubility of cleaved FL-AdPLA, and attempts to crystallize the intact MBP-FL-AdPLA protein were not successful. On the other hand, cleavage of purified MBP-T-AdPLA with TEV protease produced a soluble protein. The protein was confirmed as T-AdPLA by MS/MS analysis (supplemental Fig. S3). The purified T-AdPLA protein is monomeric in solution based on its elution profile on a size exclusion chromatography column calibrated with protein standards (supplemental Fig. S3). Crystallization screens of T-AdPLA produced small crystals in several conditions. The crystals were indexed as trigonal/hexagonal with $a = 60.05$ Å and $c = 74.06$ Å unit cell parameters. Analysis of the axial reflections indicated the presence of a 3-fold screw axis as systematic absences $00l$; $l = 3n$ were observed.

The structure solution of T-AdPLA was carried out by molecular replacement with Phaser (41) using the NMR model (Protein Data Bank code 2KYT) of AdPLA as the search model (35, 53). The terminal ends and residues 39–55 were truncated in the search model as they were shown to be disordered in Protein Data Bank code 2KYT. The top solution was obtained for a single monomer in the asymmetric unit in the space group $P3_121$. Intensities were integrated and scaled using XDS and Scala (54), respectively (Table 1). The Wilson *B*-factor was unusually high (~65 Å^2) for data processed to this resolution (2.3 Å). Because of the anisotropy of the diffraction data, the observed electron density maps were not clear in certain regions of the polypeptide chain, making it difficult to discern certain side chains. Therefore, a second data set was collected at a longer wavelength ($\lambda = 1.7463$ Å), and phased anomalous difference electron density maps were calculated in an effort to confirm the position of the Cys sulfur atoms and ensure that the sequence register was correctly assigned. Indeed, anomalous difference map peaks were observed greater than 4σ for the two Cys residues Cys^{89} and Cys^{113}, respectively (Fig. 1) The structure reported here was deposited in the Protein Data Bank under accession code 4FA0.

Overall, the structure is similar to the solution NMR structure of AdPLA (Protein Data Bank code 2KYT) with a root mean square deviation of 1.43 Å between Cα atoms (Pro^6 to Val^{124}) as determined using secondary structure matching (55) via the CCP4 interface (56) (Fig. 2). Residues between Pro^{39} and Lys^{57} were disordered and could not be fit to the electron density maps. The largest deviations between the AdPLA crystal structure and the solution NMR structure are observed in regions containing loops 27–33, 71–74, 79–87, and 106–112 as shown in Fig. 3, *A* and *C*. The crystal structure we describe here also closely resembles the one recently reported by Golczak *et al.* (20) of an AdPLA protein shorter by two amino acids at its C terminus (Protein Data Bank code 4DOT) with a root mean square deviation of 0.54 Å between Cα atoms (Pro^6 to Val^{124}). The main difference between the crystal structure reported by Golczak *et al.* (20) and the one reported here occurs in a loop region between Val^{104} and Ser^{110} as shown in Fig. 3, *B* and *C*. This difference could be attributed to the relatively high conformational flexibility of the Val^{104}–Ser^{110} loop as observed

TABLE 1
Crystallographic data for AdPLA refined to 2.65-Å resolution

	AdPLA
Data collection	
Unit cell parameters (Å)	$a = 59.99$, $c = 74.01$
Space group	$P3_121$
Resolution (Å)[a]	74.01–2.30 (2.39–2.30)
Wavelength (Å)	1.0000
Temperature (K)	100
Observed reflections	30,627
Unique reflections	7,196
$I/\sigma(I)$[a]	14.6 (2.3)
Completeness (%)[a]	99.9 (99.9)
Multiplicity[1]	4.3 (4.4)
R_{merge} (%)[a,b]	5.2 (43.7)
R_{meas} (%)[a,c]	6.0 (49.7)
R_{pim} (%)[a,c]	2.8 (23.2)
Refinement	
Resolution (Å)	30.14–2.65
Reflections (working/test)	4,743/227
R_{factor}/R_{free} (%)[d]	20.6/24.7
No. of atoms	802
Model quality	
r.m.s.[e] deviations	
Bond lengths (Å)	0.010
Bond angles (°)	1.050
Average *B*-factor (Å^2)	
All atoms	68.8
Wilson plot	65.0
Coordinate error, Luzatti plot (Å)	0.37
Ramachandran plot	
Most favored (%)	97.9
Additionally allowed (%)	2.1

[a] Values in parenthesis are for the highest resolution shell.
[b] $R_{merge} = \Sigma_{hkl}\Sigma_i|I_i(hkl) - I(hkl)|/\Sigma_{hkl}\Sigma_i I_i(hkl)$ where $I_i(hkl)$ is the intensity measured for the *i*th reflection and $I(hkl)$ is the average intensity of all reflections with indices *hkl*.
[c] R_{meas} = redundancy-independent (multiplicity-weighted) R_{merge} (39, 54). R_{pim} = precision-indicating (multiplicity-weighted) R_{merge} (87, 88).
[d] $R_{factor} = \Sigma_{hkl}||F_{obs}(hkl)| - |F_{calc}(hkl)||/\Sigma_{hkl}|F_{obs}(hkl)|$; R_{free} is calculated in an identical manner using 5% of randomly selected reflections that were not included in the refinement.
[e] Root mean square.

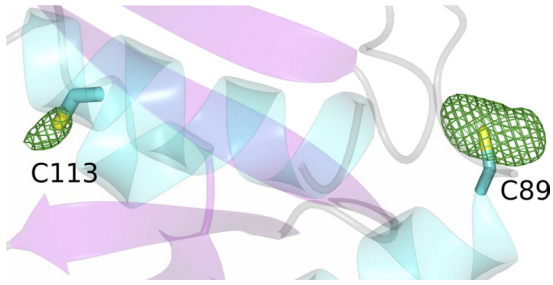

FIGURE 1. **Phase anomalous difference map (*green mesh*) contoured at 4σ using diffraction data collected at $\lambda = 1.7463$ Å.** The largest peaks were observed near Cys residues 89 and 113.

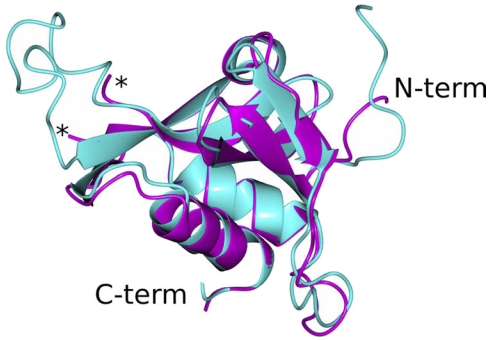

FIGURE 2. **Superposition of AdPLA structures determined by NMR (Protein Data Bank code 2KYT; colored *cyan*) and x-ray crystallography (Protein Data Bank code 4FA0; colored *magenta*).** The N- and C-terminal (*term*) ends are noted, and the disordered loop in the crystal structure is indicated by the *asterisks*.

in the values of the average *B*-factors for the residues encompassing this domain (Fig. 3*D*).

The crystal structure of AdPLA reported here (Protein Data Bank code 4FA0) reveals an $\alpha+\beta$ fold composed of three α-helices and five antiparallel β-sheets in a circular permutation of the topology of papain and members of the NlpC/P60 superfamily of cysteine peptidases (31) (Fig. 4). A Cys residue (Cys^{113}), which is highly conserved in both LRAT family proteins and the NlpC/P60 superfamily of proteins, is found on helix α3. In AdPLA and all LRAT-like proteins studied thus far, the conserved Cys^{113} residue was shown to be required for their catalytic activity (10, 14, 22) by acting as a nucleophile in forming the covalent acyl enzyme intermediate (20, 34). Our model indicates the presence of a well conserved His residue (His^{23}) on a neighboring β-strand that is 3.6 Å from Cys^{113}. A second His (His^{35}), which resides on an adjacent β-strand, is positioned 3 Å from His^{23}. The three Cys^{113}-His^{23}-His^{35} residues comprising the catalytic triad of AdPLA are found in a conserved arrangement in the active site of NlpC/P60 proteins, such as *E. coli* Spr (32).

The Residues Comprising the Catalytic Triad Are Required for the Activity of AdPLA—We assayed the contribution of the C-terminal transmembrane domain to the phospholipase activity of AdPLA. For this, we examined the activity of MBP-FL-AdPLA and MBP-T-AdPLA proteins using a continuous assay based on monitoring the release of a fluorescently labeled acyl group from the PLA_2-specific substrate BODIPY PC-A2 (the structure is depicted in Fig. 5, *top panel*). Release of the BODIPY FL pentanoic acid acyl chain from *sn*-2 of BODIPY PC-A2 results in an increase in the fluorescence signal (excitation, 488 nm; emission, 515 nm) due to decreased intramolecular quenching by fluorescence resonance energy transfer (FRET) of the BODIPY 558/568 dye attached at the *sn*-1 position. The assay allowed us to conduct a sensitive kinetic assay of AdPLA and to calculate its V_{max} (2.5 ± 0.2 μmol/min/mg) and K_m (0.7 ± 0.15 μM) using BODIPY PC-A2 as a substrate. These values are within the range of reported values for AdPLA in previous studies (10, 14). To account for the interfacial mechanism of the PLA_2-catalyzed reaction, other kinetic models, such as the "surface dilution model" (57, 58), have been developed, but we were not successful in adapting the assay based on detergent-phospholipid mixed micelles to the analysis of the MBP-FL-AdPLA reaction. In conclusion, our findings establish that MBP-FL-AdPLA exhibits characteristics consistent with a physiological role of AdPLA in the hydrolysis of phospholipids.

Next, we used site-directed mutagenesis to examine the effect of mutating the active site residues Cys^{113}, His^{23}, and His^{35} on the phospholipase activity of AdPLA. Substituting either Cys^{113}, His^{23}, or His^{35} with alanine or the more sterically conserved substitutions C113S, H23Q, and H35Q resulted in a significantly reduced AdPLA activity of the resulting proteins (Fig. 6). Both Cys^{113} and His^{23} (His^{21} in mouse AdPLA) had been previously implicated to be important for the activity of AdPLA (10, 14). Here, we also demonstrate that His^{35} is required for AdPLA activity. We propose that the function of His^{23} is to form an ion pair with Cys^{113}, acting as a base and subsequently as an acid in the reaction cycle. Meanwhile, His^{35} maintains His^{23} in its proper orientation as shown for the NlpC/P60 protein Spr (32). Thus, our studies provide experimental support for the requirement of the Cys^{113}, His^{23}, and His^{35} residues in the enzymatic activity of AdPLA.

Lack of the C-terminal Domain Impairs the Association of AdPLA with Membranes—Our results indicate that deletion of the C-terminal transmembrane domain of AdPLA severely affects the activity of MBP-T-AdPLA against liposome substrates. Using a liposome-based assay of AdPLA activity, we were not able to detect any hydrolytic activity associated with MBP-T-AdPLA (Fig. 6) or T-AdPLA (not shown). In comparison, MBP-FL-AdPLA had a robust activity (specific activity of 720 pmol/min/mg) (Fig. 6). These results are in agreement with the requirement of an intact C-terminal domain for the activity of AdPLA demonstrated by other studies (10, 14). Thus, the hydrophobic C-terminal domain is necessary for interfacial catalysis by AdPLA.

In recently published findings, Golczak *et al.* (20) examined the structure and activity of a 1–132 fragment of AdPLA with nearly the same sequence and structure as the T-AdPLA protein described here (Fig. 3, *B* and *C*). Although MBP-T-AdPLA, T-AdPLA, and His_6-AdPLA(1–132) do not display significant activity against phospholipids embedded in liposomes (results not shown), it was shown that His_6-AdPLA(1–132) protein can become acylated in the presence of phospholipids with very short fatty acid chains, such as diheptanoyl-PC (20). These findings suggest that the C-terminal domain of AdPLA does not include residues that participate in the catalytic reaction; however, this domain is required for the association of AdPLA with membranes.

Amide Hydrogen/Deuterium Exchange Dynamics of MBP-FL-AdPLA, MBP-T-AdPLA, and T-AdPLA—To shed light on the structural differences between T-AdPLA, MBP-T-AdPLA, and MBP-FL-AdPLA, we used a DXMS approach to probe the solvent accessibility of backbone amides of T-AdPLA, MBP-T-AdPLA, and MBP-FL-AdPLA. We incubated purified T-AdPLA, MBP-T-AdPLA, and MBP-FL-AdPLA with buffer supplemented with D_2O. Aliquots of the hydrogen/deuterium exchange reaction were quenched, digested with pepsin, and analyzed by LC-MS/MS. Pepsin digestion of the denatured T-AdPLA, MBP-T-AdPLA, and MBP-FL-AdPLA proteins resulted in a complete coverage of the AdPLA protein based on the identification of 36 and 30 peptides derived from the FL-AdPLA or the T-AdPLA fusion partner, respectively. The

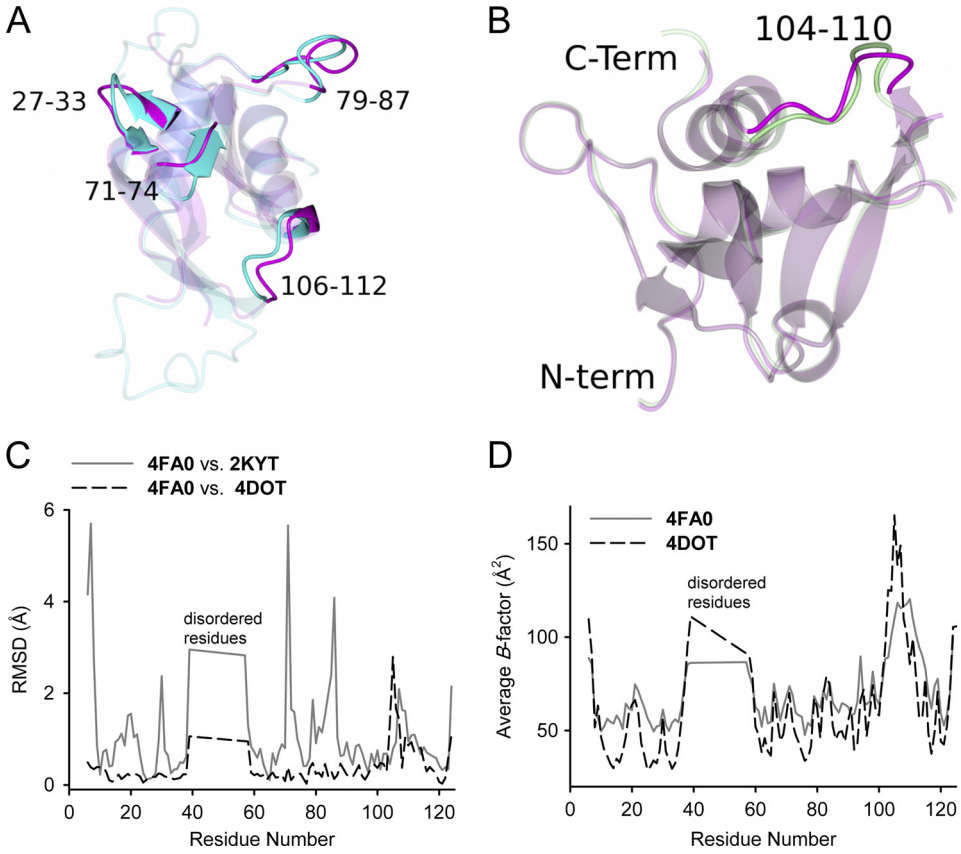

FIGURE 3. **Comparison of the NMR (Protein Data Bank code 2KYT) and x-ray structures (Protein Data Bank codes 4DOT and 4FA0) of AdPLA.** *A*, loop regions 27–33, 71–74, 79–87, and 106–112 in AdPLA structures determined by NMR (Protein Data Bank code 2KYT; colored *cyan*) and x-ray crystallography (Protein Data Bank code 4FA0; colored *magenta*) show the largest difference between the two structures. *B*, loop region 104–110 contains the largest differences between the AdPLA crystal structure reported here (Protein Data Bank code 4FA0; colored *magenta*) and the previously reported structure (Protein Data Bank code 4DOT; colored *green*). *C*, plot of root mean square deviations (*RMSD*) between Cα atoms of Protein Data Bank code 2KYT *versus* Protein Data Bank code 4FA0 (*solid gray line*) and Protein Data Bank code 4DOT *versus* Protein Data Bank code 4FA0 (*dashed black line*) models of the AdPLA. *D*, plot of average *B*-factors values of Protein Data Bank code 4DOT (*dashed black line*) and Protein Data Bank code 4FA0 (*solid gray line*).

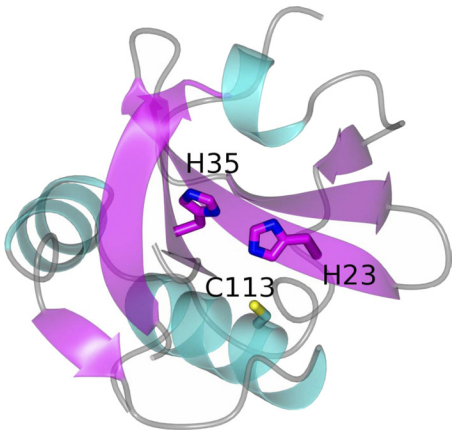

FIGURE 4. **Crystal structure of AdPLA colored by secondary structure and showing the Cys^{113}-His^{23}-His^{35} catalytic triad.**

peptides with the best signal to noise ratio and least overlapping regions for representation of the hydrogen/deuterium exchange data are shown in supplemental Fig. S4. The kinetics of the rates of deuteration of T-AdPLA, MBP-T-AdPLA, and MBP-FL-AdPLA show the same behavior with the exchange steadily increasing with time, consistent with the premise that the FL-AdPLA and T-AdPLA proteins have similar structures (Fig. 7*A*). Comparison of the exchange rates of MBP-T-AdPLA and T-AdPLA showed a similar rate of solvent accessibility, arguing that the presence of the MBP fusion partner does not affect the folding of T-AdPLA. The rates of deuteration are also consistent with the crystal structure model as shown in Fig. 7, *A* and *B*. Residues 39–59 were found to be disordered in the crystal structure and could not be modeled. Using DXMS, we observed high rates of hydrogen/deuterium exchange for the region 39–59 (greater than 80% in 10 s and reaching a maximum after 1,000 s). These fast rates of exchange reflect the inherent flexibility of the region encompassing residues 39–59. The α3 helix (residues 111–121) containing the Cys^{113} catalytic residue is packed tightly against the β-sheet β2 and thus displays relatively low rates of exchange in T-AdPLA, MBP-T-AdPLA, and MBP-FL-AdPLA. We noticed very subtle differences between MBP-FL-AdPLA *versus* MBP-T-AdPLA or T-AdPLA as the rates of deuteration for α3 appear to be slightly lower in the case of MBP-FL-AdPLA than those observed for MBP-T-AdPLA or T-AdPLA, perhaps indicating a more compact structure of this domain.

Two domains of AdPLA encompassing residues Ile^{16}–Tyr^{27} and Tyr^{66}–Glu^{98} display much lower rates of solvent accessibility compared with the rest of the protein (Fig. 7, *A* and *B*, colored *green*). Both domains also display low conformational flexibility based on average *B*-factors (Fig. 3*D*). These results are

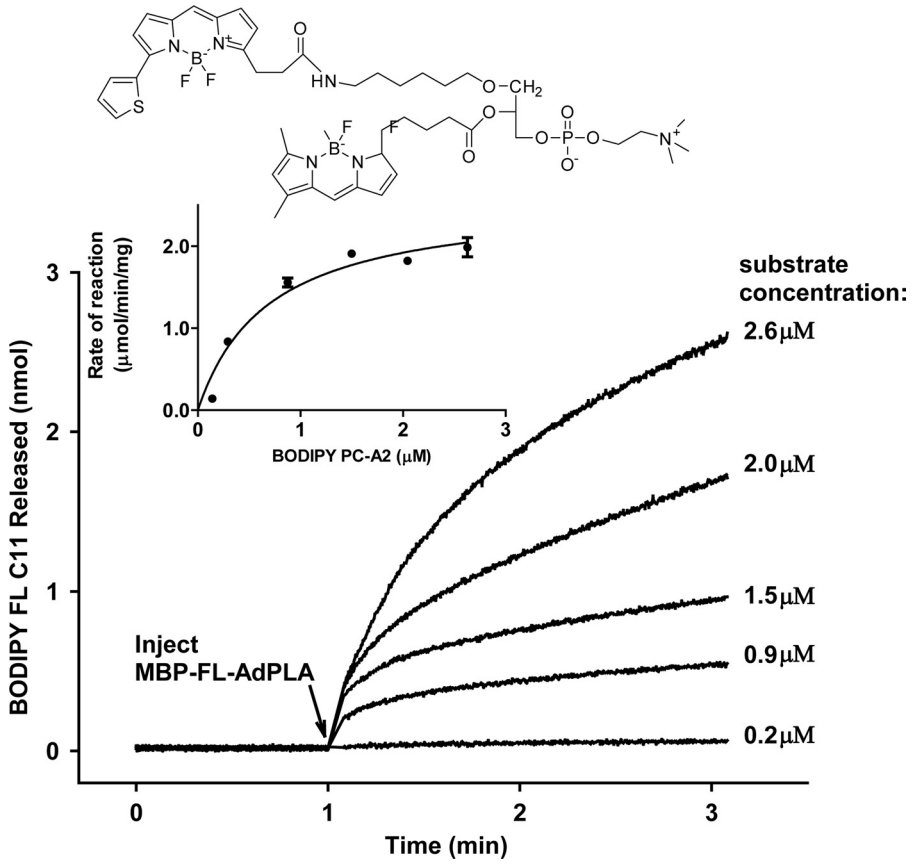

FIGURE 5. **Phospholipase A_2 activity of MBP-FL-AdPLA.** BODIPY PC-A2 was used to measure the rate of reaction as a function of substrate concentration. The 488/515 nm fluorescence signal of liposomes containing various concentrations of BODIPY PC-A2 substrate (structure shown in *top panel*) was recorded for 1 min to monitor the background emission. No significant increase in background fluorescence emission was observed. Purified MBP-FL-AdPLA protein was injected at 1 min (indicated by *arrow*), and the fluorescence signal at 488/515 nm was recorded for the next 4 min. A standard curve of BODIPY FL C5, the cleavage product of BODIPY PC-A2, was used for evaluating the amount of product formed by MBP-FL-AdPLA-mediated hydrolysis. Representative enzyme reaction progress curves are shown in the *bottom panel*. The *inset* shows the initial rates of reaction as a function of substrate concentration. Data represent means ± S.E. (*error bars; n* = 3). The enzyme kinetic data were analyzed through sum-of-squares non-linear regression to derive the V_{max} and K_m.

consistent with the tight packing around the Ile^{16}–Tyr^{27} domain, which includes the β-sheet $\beta 2$ and the His^{23} catalytic residue. In addition, the Tyr^{66}–Glu^{98} domain of AdPLA adopts a compact structure that excludes water, consistent with a possible role of this domain in additional interactions with the membrane interface. Overall, the T-AdPLA, MBP-T-AdPLA, and MBP-FL-AdPLA proteins appear to have similar solvent accessibility and to adopt similar conformations.

FL-AdPLA Displays Combined PLA_1 and PLA_2 Activities—AdPLA was initially identified as a PLA_2 enzyme (10); however, later reports suggested that the PLA_1 activity of AdPLA is in fact higher than its PLA_2 activity (14). The positional specificity, *sn*-1 *versus sn*-2 of AdPLA, is important for evaluating its physiological role. In physiological settings, unsaturated fatty acids, such as arachidonic acid, are found primarily in the *sn*-2 position of phospholipids. Arachidonic acid release is the key argument in explaining the physiological role of AdPLA in PGE_2 production; therefore, determining the positional specificity of AdPLA is essential for explaining its physiological function.

The process of determining the positional specificity of phospholipases is affected by the rapid intramolecular rearrangement of lysophospholipids. Following cleavage by PLA_1, the 2-acyl lyso-PC product rearranges to form the more thermodynamically favored 1-acyl lyso-PC (59). Subsequent action of PLA_1 can result in a second round of hydrolysis and the production of L-α-glycerylphosphorylcholine through the release of the migrated acyl group. Thus, both *sn*-1- and *sn*-2-derived fatty acids can be released by a PLA_1 enzyme despite its specificity for the *sn*-1 position of phospholipids. Because AdPLA was reported to release both *sn*-1 and *sn*-2 fatty acids, we sought to determine whether the combined PLA_1/PLA_2 activity could be explained by PLA_1 activity alone.

Based on a fluorescence-based continuous assay using BODIPY PC-A2, our data argue that AdPLA displays intrinsic PLA_2 activity by accessing the *sn*-2 acyl group directly. As seen in Fig. 5, MBP-FL-AdPLA can hydrolyze the BODIPY PC-A2, resulting in the increase of the fluorescence of the BODIPY FL dye. Because the mechanism of detection in this assay depends on the reduced quenching of the BODIPY FL dye by FRET of BODIPY 558/568, this implies that either the *sn*-1 or *sn*-2 labeled probes of BODIPY PC-A2 were hydrolyzed and released by MBP-FL-AdPLA. BODIPY PC-A2 contains an alkyl group linked through an ether bond in the *sn*-1 position. The ether bond of BODIPY PC-A2 confers PLA_2 specificity by virtue of the fact that AdPLA, like most other PLA_2 enzymes, does not hydrolyze ether bonds as found in 18:0-18:0 diether PC (results not shown). Together, these results demonstrate that

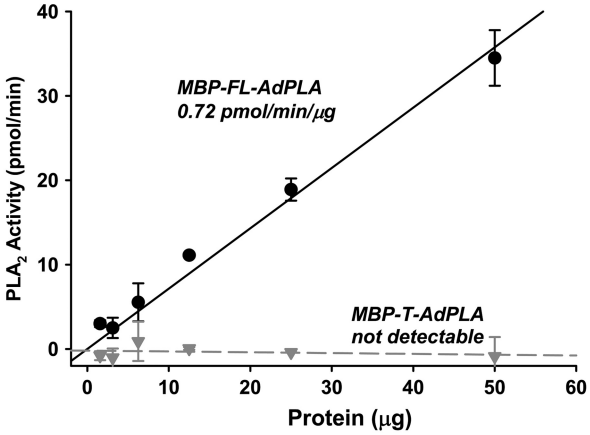

PLA_2 Activity of MBP-FL-AdPLA Active Site Mutants					
Mutant	**H23A**	**H23Q**	**H35A**	**H35Q**	**C113S**
Activity (% wild type)	2.8±0.3	2.7±0.7	2.8±1.0	3.0±0.7	1.4±0.7

FIGURE 6. **Deletion and mutagenesis analysis of MBP-FL-AdPLA.** *Top panel*, rate of reaction of MBP-FL-AdPLA and MBP-T-AdPLA as a function of enzyme concentration. The rate of PLA_2 activity of MBP-FL-AdPLA and MBP-T-AdPLA was measured during steady-state conditions using the fluorescent substrate BODIPY PC-A2. A standard curve of BODIPY FL C5 was used for evaluating the amount of product formed by MBP-FL-AdPLA-mediated hydrolysis. Data represent means ± S.E. (*error bars; n* = 3). *Bottom panel*, the rate of activity of wild type and active site mutants of MBP-FL-AdPLA. Equal amounts of purified recombinant proteins were examined for hydrolysis of BODIPY PC-A2. The rate of activity is expressed as a percentage of the activity of wild type protein.

the release of the BODIPY FL pentanoic acid acyl chain from *sn*-2 of BODIPY PC-A2 is the result of direct hydrolysis of the *sn*-2 ester bond by MBP-FL-AdPLA and that MBP-FL-AdPLA has authentic PLA_2 activity.

It is important to determine the specificity of AdPLA for physiological substrates incorporated in liposomes that resemble the composition of cellular membranes. Thus, we used a secondary method to assess the activity of MBP-FL-AdPLA using a direct assay of the hydrolysis of natural phospholipid substrates. To determine the PLA_1 or PLA_2 specificity of MBP-FL-AdPLA, we used PC substrates with mixed acyl chains. We incubated MBP-FL-AdPLA, MBP-T-AdPLA, commercial PLA_2 (bee venom), or PLA_1 (*T. lanuginosus* lipase) preparations with liposomes composed of an equimolar mix of 18:1-18:1 PG and various species of PC. We then extracted and examined the fatty acids produced by HPLC using charged aerosol detection.

Our results indicate that MBP-FL-AdPLA displays potent PLA_1 and PLA_2 activities by catalyzing the hydrolysis of roughly equivalent amounts of stearate (18:0) or palmitate (16:0) whether linked to the *sn*-1 or the *sn*-2 position of 16:0-18:0 PC or 18:0-16:0 PC (Fig. 8, *A* and *B*). In the case of phospholipids containing unsaturated acyl chains, MBP-FL-AdPLA hydrolyzed the release of slightly more palmitate from the *sn*-1 position of 16:0-20:4 PC or 16:0-18:2 PC than arachidonate (20:4) or linoleate (18:2) from the *sn*-2 position, respectively (Fig. 8, *D* and *E*). To confirm the specificity of the substrates, we examined the hydrolysis of PC species with mixed acyl groups using authentic PLA_1 or PLA_2 enzyme preparations. By incubating liposomes composed of PC species with mixed acyl groups with the PLA_1 enzyme from *T. lanuginosus*, we observed the release of fatty acids linked predominantly to the *sn*-1 position in 18:0-16:0 PC (Fig. 8*C*) or 16:0-18:0 PC (not shown). Meanwhile, hydrolysis of PC species with mixed acyl groups by PLA_2 resulted in the release of fatty acids linked to the *sn*-2 position of 18:0-16:0 PC (Fig. 8*C*) and 16:0-18:0 PC (not shown). Comparison of the rates of hydrolysis indicates that MBP-FL-AdPLA does not appear to show any preference for the hydrolysis of arachidonic acid. Our results also show that MBP-FL-AdPLA can hydrolyze PG to release oleate (18:1) (Fig. 8*F*), indicating that additional phospholipid headgroups other than aminophospholipids can be recognized by AdPLA. As predicted, based on the fluorescent AdPLA assays, the levels of fatty acids measured in all assays of MBP-T-AdPLA activity are equivalent to the buffer control reaction; and therefore, MBP-T-AdPLA does not exhibit significant hydrolytic activity against substrates embedded in liposomes (Fig. 8). In conclusion, our data presented in Figs. 6 and 8 support a model in which AdPLA has combined PLA_1 and PLA_2 activities as opposed to exclusively PLA_1 or PLA_2 activity.

DISCUSSION

Our findings describe the structure and enzymatic activity of AdPLA, an enzyme that plays an important role in the regulation of adipose tissue function. To gain a better understanding of the molecular mechanism of AdPLA, we solved the crystal structure of a soluble fragment of AdPLA to 2.65-Å resolution (Protein Data Bank code 4FA0). The model presented here closely resembles the previously reported NMR model (Protein Data Bank code 2KYT) (Figs. 2 and 3, *A* and *C*) and the crystal structure model of AdPLA (Protein Data Bank code 4DOT) (Fig. 3, *B* and *C*). The model indicates that AdPLA adopts a globular fold consisting of three α-helices and five antiparallel β-sheets (Fig. 4) organized in a circular permutation of the classic papain fold. AdPLA utilizes a conserved Cys-His-His catalytic triad to orchestrate the nucleophilic attack by Cys on the *sn*-1 and *sn*-2 acyl groups of phospholipids. In line with this observation, residues Cys^{113}, His^{23}, and His^{35} are required for the its activity (Fig. 6). The use of a Cys residue for catalyzing the hydrolysis of phospholipids is unique to the phospholipases and acyltransferases found in the LRAT family. For Cys^{113} to act as a nucleophile, it would require a pK_a of less than 7.0; however, the pK_a of free Cys of roughly 8.3–8.8 cannot account for the nucleophilic character of this residue. Therefore, the active site of AdPLA provides an environment that is critical for catalysis by decreasing the pK_a of Cys^{113}. In papain, such function is provided by a His residue positioned 3.01 Å from the active thiol to form a thiolate-imidazolium ion pair (60, 61). Based on the similarity of AdPLA to papain, we propose that His^{23} assists in the deprotonation of Cys^{113}. The distance from the Nϵ of His^{23} to the Sγ of Cys^{113} is greater than that generally observed in other proteins utilizing a Cys-His pair; nevertheless, the role of the His^{23}-Cys^{113} ion pair in the catalytic mechanism of AdPLA is supported by the abolished activity of the H23A and H23Q mutants (Fig. 6). We cannot rule out that additional residues or the dipole of the α3 helix (62) could also interact with Cys^{113} and contribute to its reduced pK_a to generate a strong enough nucleophile.

To explore the enzymatic activity of AdPLA, we generated an MBP-fused, full-length recombinant form of AdPLA, MBP-FL-

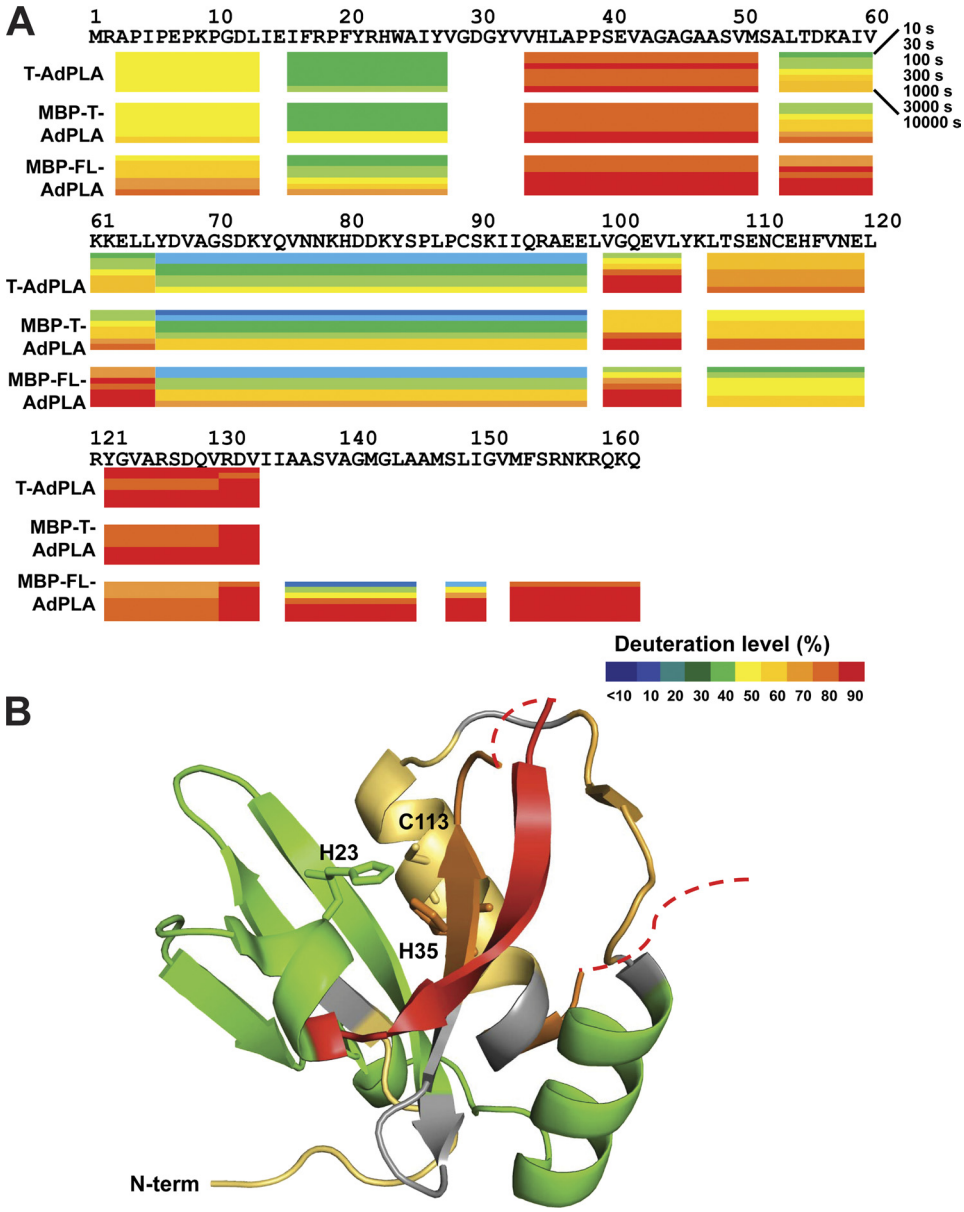

FIGURE 7. **Amide hydrogen/deuterium exchange analysis of T-AdPLA, MBP-T-AdPLA, and MBP-FL-AdPLA.** *A*, the percentage of maximal deuterium incorporation in T-AdPLA (*upper* ribbon), MBP-T-AdPLA (*middle* ribbon), and MBP-FL-AdPLA (*lower* ribbon) peptidic regions is shown. In each ribbon, the percentage of deuteration at each of the labeling durations is shown from 10 to 10,000 s (*top* to *bottom*). Differential coloring indicates the percentage of maximal labeling in a given time point. *B*, crystal structure of AdPLA colored based on fast (*red*) or intermediate (*green*) hydrogen/deuterium exchange rates. The N terminus and the residues His^{23}, His^{35}, and Cys^{113} composing the catalytic triad are indicated. *Dotted lines* represent the C-terminal strands and the 35–59 loop region for which there are no x-ray data.

AdPLA, which exhibits robust PLA_1 and PLA_2 activities against natural substrates (Fig. 8). We characterized the activity of MBP-FL-AdPLA using a continuous fluorescence-based assay, and we observed enzyme kinetics consistent with a physiologically relevant PLA enzyme (Fig. 5). The use of a fluorescent substrate containing a non-hydrolyzable bond in the *sn*-1 position provides additional support for the intrinsic PLA_2 activity of AdPLA (Fig. 5). In addition to the residues involved in catalysis, we determined that the transmembrane domain of AdPLA is also required for interfacial catalysis. As a result, MBP-T-AdPLA and T-AdPLA, which are recombinant fragments of AdPLA that lack the transmembrane domain, have no detectable PLA_1/PLA_2 activity against liposome substrates (Figs. 6 and 8).

We probed the solvent accessibility of backbone amides of MBP-FL-AdPLA, T-AdPLA, and MBP-T-AdPLA using a DXMS approach. The Tyr^{66}–Glu^{98} domain shows low rates of hydrogen/deuterium exchange consistent with the tight globular packing around the β-sheet β2 (Fig. 7, *A* and *B*). On the other hand, the residues that surround the active site of AdPLA display relatively high rates of hydrogen/deuterium exchange (Fig. 7*B*). Thus, we propose that in the process of catalysis water can readily access the active site of AdPLA and allow the acyl enzyme-thioester intermediate to decompose to free fatty acid and lysophospholipid. In agreement with this mechanism, AdPLA displays a robust PLA_2 activity rather than an exclusive acyltransferase activity as observed in the case of LRAT. Anal-

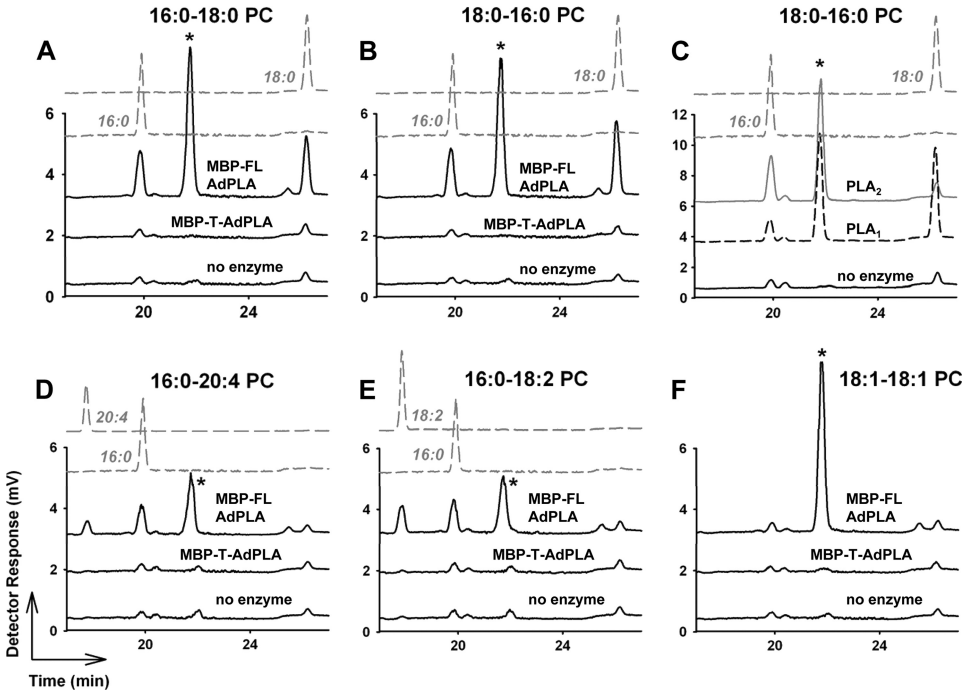

FIGURE 8. **Analysis of the specificity of the phospholipase activity of MBP-FL-AdPLA and MBP-T-AdPLA.** PLA_1/PLA_2 activity was assayed using liposome compositions containing an equimolar mixture of 18:1-18:1 PG and one of five different PC species examined as indicated at the *top* of each panel. The liposomes were incubated for 15 min with either MBP-FL-AdPLA, MBP-T-AdPLA, buffer control (labeled *no enzyme*), bee venom PLA_2, or PLA_1 from *T. lanuginosus* (*C*). The resulting fatty acids were extracted and analyzed by HPLC-charged aerosol detection. The fatty acid products of reactions carried out (*solid black line* chromatograms) were identified based on the elution profile in comparison with authentic standards (*dashed gray line* chromatograms). The oleate (18:1) fatty acid product of the hydrolysis of 18:1-18:1 PG (*A–F*) or 18:1-18:1 PC (*F*) by MBP-FL-AdPLA, bee venom PLA_2, or PLA_1 from *T. lanuginosus* is indicated by a *black star* (*). The experiment was conducted in triplicate and repeated.

ysis of MBP-FL-AdPLA, MBP-T-AdPLA, and T-AdPLA by DXMS also indicates that there are no large changes in conformation between the different forms of the AdPLA protein; thus, it is likely that the structure we report for T-AdPLA resembles the catalytically active MBP-FL-AdPLA protein (Fig. 7), and we attribute the lack of interfacial catalysis by MBP-T-AdPLA and T-AdPLA to the absence of a membrane targeting domain.

Membrane Targeting of AdPLA—The association of AdPLA with membranes is an essential part of the interfacial catalysis process. With the exception of several calcium-independent PLA_2s, such as Group VIC PLA_2 (patatin-like phospholipase domain-containing 6 (PNPLA6) (63) and patatin-like phospholipase domain-containing 7 (PNPLA7) (64, 65), most PLA_2 enzymes characterized so far are soluble. Generally, secreted PLA_2 and Group IVA cytosolic PLA_2 target the phospholipid bilayer in response to signals, such as binding of calcium. Other PLA_2s, like group VI A PLA_2 (calcium-independent $PLA_2\beta$) or lipoprotein-associated PLA_2, are targeted to the membrane via hydrophobic pockets (66, 67). In contrast to most PLA_2 enzymes, AdPLA is an integral membrane protein. Like the related tazarotene-induced gene 3 (68) and LRAT proteins (69), AdPLA is targeted to membranes via a C-terminal signal anchor domain to assume a "tail-anchored" membrane topology (10, 51). Truncated AdPLA lacking the membrane-spanning C-terminal domain is not active against phospholipids embedded in liposomes (reported here and in Refs. 10 and 14) as it does not associate with membranes (10). By virtue of the targeting signal being the last domain to exit the ribosome, tail-anchored proteins must be targeted to membranes in a post-translational fashion, *i.e.* after protein translation has been completed (70). A substantial fraction of AdPLA is found to be localized in the cytosol (51). Thus, post-translational translocation of AdPLA could allow AdPLA to be targeted to subcellular compartments that have different lipid pools, such as the endoplasmic reticulum or peroxisomes (22), and play a role in its mechanism of action.

Relationship of AdPLA to NlpC/P60 Enzymes—The structure of AdPLA, the first member of the LRAT family to be structurally characterized (model presented here and in Refs. 20 and 35), appears to be related to the papain-like NlpC/P60 bacterial cysteine peptidases that are involved in remodeling of the bacterial cell wall (31). The evolutionary relationship between the LRAT family of proteins and the NlpC/P60 protein superfamily is intriguing and could provide clues to the function of these related enzymes. For example, our results indicate that AdPLA shares the conformation of the Cys-His-His catalytic triad first described in the case of the classical NlpC/P60 protein, Spr, from *E. coli* (32). AdPLA also resembles the structure of YiiF, an NlpC/P60 permuted domain protein from *E. coli* whose structure indicates the presence of a bound stearate molecule (71). These observations suggest that eukaryotic representatives of the LRAT family of proteins are related in both structure and enzymatic mechanism to cysteine hydrolases from the NlpC/P60 family that catalyze various acylation/deacylation reactions involving proteins and lipids.

Role of AdPLA in the Regulation of Lipolysis—One of the strongest arguments in favor of a role for AdPLA in the generation of free arachidonic acid in fat is the dramatic decrease in the phospholipase A activity (18% of wild type levels) and PGE_2

levels (12% of wild type levels) in adipose tissues of *AdPLA*−/− mice compared with wild type mice (11). In addition, treatment of adipocytes isolated from *AdPLA*−/− mice with PGE_2 can restore lipolysis and cAMP to wild type levels (11). These observations are consistent with a role of AdPLA in the formation of PGE_2 in fat whereby *AdPLA*−/− mice have a higher net rate of adipose tissue lipolysis as a result of decreased prostaglandin E receptor 3 signaling (11). However, the robust PLA_1 activity of AdPLA brings into question its role in the release of arachidonic acid as this fatty acid is generally bound to the *sn*-2, not the *sn*-1, position of phospholipids.

In addition to PLA_1 and PLA_2 activities, it was reported that AdPLA also displays *N*-acylation activity (14, 20), suggesting that it might have a potential role in the formation of *N*-acylphosphatidylethanolamine, a precursor of endocannabinoids, an important class of endocrine regulators (20). Nevertheless, AdPLA displays very low *N*-acylation activity (results not shown and Ref. 19) in comparison with the PLA_1/PLA_2 activities described here and elsewhere (10, 14) that suggest that in a cellular environment fatty acid hydrolysis would occur more often than acyl transfer to phosphatidylethanolamine. However, we cannot exclude the possibility that AdPLA contributes to the synthesis of endocannabinoid precursors in fat or that there might still be other unidentified acyl acceptors that become esterified by AdPLA.

Other products of the AdPLA-mediated hydrolysis besides free fatty acids could have important regulatory roles in fat. Our studies show that AdPLA is a potent combined PLA_1/PLA_2 enzyme, leading to the release of free fatty acids and the formation of 2- or 1-lysophospholipids, respectively. In our studies, AdPLA displays very low lysophospholipase activity and thus does not further hydrolyze lysophospholipids to generate L-α-glycerylphosphorylcholine (results not shown and Refs. 10 and 14). Lysophospholipids can become precursors to important bioactive lipid mediators, such as lysophosphatidic acid (LPA) through the action of lysophospholipase D/autotaxin (72). LPA can in turn be acylated by either comparative gene identification-58 (CGI-58) or adiponutrin to produce phosphatidic acid (73–75). Because AdPLA, autotaxin, CGI-58, and adiponutrin are highly expressed in adipose tissue (10, 76–79), the contribution of AdPLA to the formation of LPA or phosphatidic acid in adipose tissue is particularly pertinent. Phosphatidic acid is a central lipid signaling mediator in fat as seen in both the resistance to obesity of CGI-58 knockdown mice (80) and the lipodystrophy seen in patients suffering from Chanarin-Dorfman syndrome due to CGI-58 deficiency (81–83). LPA in its own right is a potent inducer of white adipose tissue formation and a negative regulator of thermogenic, brown fat (84). Mice deficient in the LPA receptor LPA1R are resistant to diet-induced obesity (85). Similarly, *AdPLA*−/− are lean, and the white adipose tissue of *AdPLA*−/− mice displays increased thermogenesis and fatty acid oxidation (11), which is consistent with the possibility that *AdPLA*−/− mice have decreased levels of LPA. This is an attractive hypothesis because it offers an explanation for a role of AdPLA in adipose tissue that is independent of the formation of PGE_2. This hypothesis also fits with the lack of positional or acyl chain specificity of AdPLA. The role of AdPLA in the generation of LPA could be explored by examining the levels of LPA and the activation of cognate LPA receptors in the tissues of *AdPLA*−/− and wild type mice.

Conclusion—We solved the structure of AdPLA, leading us to the identification of the Cys-His-His residues involved in the catalytic activity of AdPLA. Our results demonstrate that the Cys-His-His catalytic triad and the signal anchor domain of AdPLA are both required for its function. We describe the purification of a recombinant form of full-length AdPLA, which we characterize as a combined PLA_1/PLA_2 enzyme. The potent PLA_1 activity exhibited by AdPLA suggests that other products of AdPLA-mediated hydrolysis other than arachidonic acid could also play a role in its antilipolytic effects.

Recent developments in the understanding of the physiological role, enzymology, and structure of AdPLA pave the way for the development of inhibitors of AdPLA. Such inhibitors are expected to have a positive impact on the treatment of obesity by promoting adipose tissue lipolysis and mimicking the phenotype of the *AdPLA*−/− mice. Although this goal makes AdPLA an attractive therapeutic target in obesity settings, an important caveat is that unchecked lipolysis could lead to ectopic lipid accumulation if not compensated by increased fatty acid oxidation. As a consequence, both *AdPLA*−/−,*ob*/*ob* double knock-out mice and *AdPLA*−/− mice on a high fat diet exhibit hepatic lipid accumulation and resistance to insulin (11). However, milder increases in lipolysis as seen in mice overexpressing adipose triglyceride lipase can improve insulin sensitivity (86). It is possible that pharmacological inhibition of AdPLA will not elicit lipolysis and ectopic lipid deposition to the same extent as in *AdPLA*−/− mice maintained on a high fat diet, particularly if treatment with AdPLA inhibitors is administered in conjunction with a low fat diet or with therapies aimed at increasing fatty acid oxidation. To achieve this goal and improve upon these first insights into the AdPLA enzymatic mechanism, the structure of AdPLA in complex with substrates or inhibitors is greatly needed. Such findings would shed light on the residues involved in the binding and substrate specificity of AdPLA. Trapping the enzyme-substrate complex would allow us to observe the formation of the presumed tetrahedral intermediate and to define the position of the oxyanion hole necessary to polarize the carbonyl group of the substrate. In parallel with structural approaches, more studies are also needed to explore the physiological role and the consequences of the disruption of AdPLA *in vivo*.

Acknowledgments—We thank Drs. Rick Dobrowsky, Hei Sook Sul, Robert Hanzlik, Jeff Staudinger, and Ross Stein for valuable discussions. We thank Sara Billings for advice and help in the preparation of the manuscript. We thank Dan Brown and Amanda Wise for help in cloning and initial assay development and Dr. Fei Philip Gao for help in designing the protein purification strategy. We thank Drs. Marcin Golczak and Krzysztof Palczewski for the gift of the pET30b-HRASLS3 bacterial expression construct. Use of the IMCA-CAT beamline 17-ID at the Advanced Photon Source was supported by the companies of the Industrial Macromolecular Crystallography Association through a contract with the Hauptman-Woodward Medical Research Institute. Use of the Advanced Photon Source was also supported by the United States Department of Energy, Office of Science, Office of Basic Energy Sciences under Contract DE-AC02-06CH11357.

REFERENCES

1. Coppack, S. W., Jensen, M. D., and Miles, J. M. (1994) *In vivo* regulation of lipolysis in humans. *J. Lipid Res.* **35,** 177–193
2. Villena, J. A., Roy, S., Sarkadi-Nagy, E., Kim, K. H., and Sul, H. S. (2004) Desnutrin, an adipocyte gene encoding a novel patatin domain-containing protein, is induced by fasting and glucocorticoids: ectopic expression of desnutrin increases triglyceride hydrolysis. *J. Biol. Chem.* **279,** 47066–47075
3. Zimmermann, R., Strauss, J. G., Haemmerle, G., Schoiswohl, G., Birner-Gruenberger, R., Riederer, M., Lass, A., Neuberger, G., Eisenhaber, F., Hermetter, A., and Zechner, R. (2004) Fat mobilization in adipose tissue is promoted by adipose triglyceride lipase. *Science* **306,** 1383–1386
4. Jenkins, C. M., Mancuso, D. J., Yan, W., Sims, H. F., Gibson, B., and Gross, R. W. (2004) Identification, cloning, expression, and purification of three novel human calcium-independent phospholipase A_2 family members possessing triacylglycerol lipase and acylglycerol transacylase activities. *J. Biol. Chem.* **279,** 48968–48975
5. Osuga, J., Ishibashi, S., Oka, T., Yagyu, H., Tozawa, R., Fujimoto, A., Shionoiri, F., Yahagi, N., Kraemer, F. B., Tsutsumi, O., and Yamada, N. (2000) Targeted disruption of hormone-sensitive lipase results in male sterility and adipocyte hypertrophy, but not in obesity. *Proc. Natl. Acad. Sci. U.S.A.* **97,** 787–792
6. Holm, C., Kirchgessner, T. G., Svenson, K. L., Fredrikson, G., Nilsson, S., Miller, C. G., Shively, J. E., Heinzmann, C., Sparkes, R. S., and Mohandas, T. (1988) Hormone-sensitive lipase: sequence, expression, and chromosomal localization to 19 cent-q13.3. *Science* **241,** 1503–1506
7. Fredrikson, G., Tornqvist, H., and Belfrage, P. (1986) Hormone-sensitive lipase and monoacylglycerol lipase are both required for complete degradation of adipocyte triacylglycerol. *Biochim. Biophys. Acta* **876,** 288–293
8. Lass, A., Zimmermann, R., Oberer, M., and Zechner, R. (2011) Lipolysis—a highly regulated multi-enzyme complex mediates the catabolism of cellular fat stores. *Prog. Lipid Res.* **50,** 14–27
9. Dennis, E. A., Cao, J., Hsu, Y. H., Magrioti, V., and Kokotos, G. (2011) Phospholipase A_2 enzymes: physical structure, biological function, disease implication, chemical inhibition, and therapeutic intervention. *Chem. Rev.* **111,** 6130–6185
10. Duncan, R. E., Sarkadi-Nagy, E., Jaworski, K., Ahmadian, M., and Sul, H. S. (2008) Identification and functional characterization of adipose-specific phospholipase A_2 (AdPLA). *J. Biol. Chem.* **283,** 25428–25436
11. Jaworski, K., Ahmadian, M., Duncan, R. E., Sarkadi-Nagy, E., Varady, K. A., Hellerstein, M. K., Lee, H. Y., Samuel, V. T., Shulman, G. I., Kim, K. H., de Val, S., Kang, C., and Sul, H. S. (2009) AdPLA ablation increases lipolysis and prevents obesity induced by high-fat feeding or leptin deficiency. *Nat. Med.* **15,** 159–168
12. Hummasti, S., Hong, C., Bensinger, S. J., and Tontonoz, P. (2008) HRASLS3 is a PPARγ-selective target gene that promotes adipocyte differentiation. *J. Lipid Res.* **49,** 2535–2544
13. Fain, J. N., Leffler, C. W., and Bahouth, S. W. (2000) Eicosanoids as endogenous regulators of leptin release and lipolysis by mouse adipose tissue in primary culture. *J. Lipid Res.* **41,** 1689–1694
14. Uyama, T., Morishita, J., Jin, X. H., Okamoto, Y., Tsuboi, K., and Ueda, N. (2009) The tumor suppressor gene H-Rev107 functions as a novel Ca^{2+}-independent cytosolic phospholipase $A_{1/2}$ of the thiol hydrolase type. *J. Lipid Res.* **50,** 685–693
15. Ruiz, A., Winston, A., Lim, Y. H., Gilbert, B. A., Rando, R. R., and Bok, D. (1999) Molecular and biochemical characterization of lecithin retinol acyltransferase. *J. Biol. Chem.* **274,** 3834–3841
16. Shinohara, N., Uyama, T., Jin, X. H., Tsuboi, K., Tonai, T., Houchi, H., and Ueda, N. (2011) Enzymological analysis of the tumor suppressor A-C1 reveals a novel group of phospholipid-metabolizing enzymes. *J. Lipid Res.* **52,** 1927–1935
17. Uyama, T., Jin, X. H., Tsuboi, K., Tonai, T., and Ueda, N. (2009) Characterization of the human tumor suppressors TIG3 and HRASLS2 as phospholipid-metabolizing enzymes. *Biochim. Biophys. Acta* **1791,** 1114–1124
18. Jin, X. H., Uyama, T., Wang, J., Okamoto, Y., Tonai, T., and Ueda, N. (2009) cDNA cloning and characterization of human and mouse Ca^{2+}-independent phosphatidylethanolamine *N*-acyltransferases. *Biochim. Biophys. Acta* **1791,** 32–38
19. Uyama, T., Ikematsu, N., Inoue, M., Shinohara, N., Jin, X. H., Tsuboi, K., Tonai, T., Tokumura, A., and Ueda, N. (2012) Generation of *N*-acylphosphatidylethanolamine by members of the phospholipase A/acyltransferase (PLA/AT) family. *J. Biol. Chem.* **287,** 31905–31919
20. Golczak, M., Kiser, P. D., Sears, A. E., Lodowski, D. T., Blaner, W. S., and Palczewski, K. (2012) Structural basis for the acyltransferase activity of lecithin:retinol acyltransferase-like proteins. *J. Biol. Chem.* **287,** 23790–23807
21. Graham, F. L., Smiley, J., Russell, W. C., and Nairn, R. (1977) Characteristics of a human cell line transformed by DNA from human adenovirus type 5. *J. Gen. Virol* **36,** 59–74
22. Uyama, T., Ichi, I., Kono, N., Inoue, A., Tsuboi, K., Jin, X. H., Araki, N., Aoki, J., Arai, H., and Ueda, N. (2012) Regulation of peroxisomal lipid metabolism by catalytic activity of tumor suppressor H-rev107. *J. Biol. Chem.* **287,** 2706–2718
23. Hajnal, A., Klemenz, R., and Schäfer, R. (1994) Subtraction cloning of H-rev107, a gene specifically expressed in H-ras resistant fibroblasts. *Oncogene* **9,** 479–490
24. Husmann, K., Sers, C., Fietze, E., Mincheva, A., Lichter, P., and Schäfer, R. (1998) Transcriptional and translational downregulation of H-REV107, a class II tumour suppressor gene located on human chromosome 11q11-12. *Oncogene* **17,** 1305–1312
25. Siegrist, S., Féral, C., Chami, M., Solhonne, B., Mattéi, M. G., Rajpert-De Meyts, E., Guellaën, G., and Bulle, F. (2001) hH-Rev107, a class II tumor suppressor gene, is expressed by post-meiotic testicular germ cells and CIS cells but not by human testicular germ cell tumors. *Oncogene* **20,** 5155–5163
26. Roder, K., Latasa, M. J., and Sul, H. S. (2002) Silencing of the mouse H-rev107 gene encoding a class II tumor suppressor by CpG methylation. *J. Biol. Chem.* **277,** 30543–30550
27. Roder, K., Kim, K. H., and Sul, H. S. (2002) Induction of murine H-rev107 gene expression by growth arrest and histone acetylation: involvement of an Sp1/Sp3-binding GC-box. *Biochem. Biophys. Res. Commun.* **294,** 63–70
28. Sers, C., Emmenegger, U., Husmann, K., Bucher, K., Andres, A. C., and Schäfer, R. (1997) Growth-inhibitory activity and downregulation of the class II tumor-suppressor gene H-rev107 in tumor cell lines and experimental tumors. *J. Cell Biol.* **136,** 935–944
29. Sers, C., Husmann, K., Nazarenko, I., Reich, S., Wiechen, K., Zhumabayeva, B., Adhikari, P., Schröder, K., Gontarewicz, A., and Schäfer, R. (2002) The class II tumour suppressor gene H-REV107-1 is a target of interferon-regulatory factor-1 and is involved in IFNγ-induced cell death in human ovarian carcinoma cells. *Oncogene* **21,** 2829–2839
30. Ishikawa, S., Hara, Y., Ohnishi, R., and Sekiguchi, J. (1998) Regulation of a new cell wall hydrolase gene, *cwlF*, which affects cell separation in *Bacillus subtilis*. *J. Bacteriol.* **180,** 2549–2555
31. Anantharaman, V., and Aravind, L. (2003) Evolutionary history, structural features and biochemical diversity of the NlpC/P60 superfamily of enzymes. *Genome Biol.* **4,** R11
32. Aramini, J. M., Rossi, P., Huang, Y. J., Zhao, L., Jiang, M., Maglaqui, M., Xiao, R., Locke, J., Nair, R., Rost, B., Acton, T. B., Inouye, M., and Montelione, G. T. (2008) Solution NMR structure of the NlpC/P60 domain of lipoprotein Spr from *Escherichia coli*: structural evidence for a novel cysteine peptidase catalytic triad. *Biochemistry* **47,** 9715–9717
33. Xu, Q., Abdubek, P., Astakhova, T., Axelrod, H. L., Bakolitsa, C., Cai, X., Carlton, D., Chen, C., Chiu, H. J., Chiu, M., Clayton, T., Das, D., Deller, M. C., Duan, L., Ellrott, K., Farr, C. L., Feuerhelm, J., Grant, J. C., Grzechnik, A., Han, G. W., Jaroszewski, L., Jin, K. K., Klock, H. E., Knuth, M. W., Kozbial, P., Krishna, S. S., Kumar, A., Lam, W. W., Marciano, D., Miller, M. D., Morse, A. T., Nigoghossian, E., Nopakun, A., Okach, L., Puckett, C., Reyes, R., Tien, H. J., Trame, C. B., van den Bedem, H., Weekes, D., Wooten, T., Yeh, A., Hodgson, K. O., Wooley, J., Elsliger, M. A., Deacon, A. M., Godzik, A., Lesley, S. A., and Wilson, I. A. (2010) Structure of the γ-D-glutamyl-L-diamino acid endopeptidase YkfC from *Bacillus cereus* in complex with L-Ala-γ-D-Glu: insights into substrate recognition by NlpC/P60 cysteine peptidases. *Acta Crystallogr. Sect. F Struct. Biol. Cryst. Com-*

mun. **66,** 1354–1364
34. Golczak, M., and Palczewski, K. (2010) An acyl-covalent enzyme intermediate of lecithin:retinol acyltransferase. *J. Biol. Chem.* **285,** 29217–29222
35. Ren, X., Lin, J., Jin, C., and Xia, B. (2010) Solution structure of the N-terminal catalytic domain of human H-REV107—a novel circular permutated NlpC/P60 domain. *FEBS Lett.* **584,** 4222–4226
36. Qin, H., Hu, J., Hua, Y., Challa, S. V., Cross, T. A., and Gao, F. P. (2008) Construction of a series of vectors for high throughput cloning and expression screening of membrane proteins from *Mycobacterium tuberculosis*. *BMC Biotechnol.* **8,** 51
37. Studier, F. W. (2005) Protein production by auto-induction in high density shaking cultures. *Protein Expr. Purif.* **41,** 207–234
38. Kabsch, W. (1988) Automatic indexing of rotation diffraction patterns. *J. Appl. Crystallogr.* **21,** 67–71
39. Evans, P. R. (2011) An introduction to data reduction: space-group determination, scaling and intensity statistics. *Acta Crystallogr. D Biol. Crystallogr.* **67,** 282–292
40. Matthews, B. W. (1968) Solvent content of protein crystals. *J. Mol. Biol.* **33,** 491–497
41. McCoy, A. J., Grosse-Kunstleve, R. W., Adams, P. D., Winn, M. D., Storoni, L. C., and Read, R. J. (2007) Phaser crystallographic software. *J. Appl. Crystallogr.* **40,** 658–674
42. Adams, P. D., Afonine, P. V., Bunkóczi, G., Chen, V. B., Davis, I. W., Echols, N., Headd, J. J., Hung, L. W., Kapral, G. J., Grosse-Kunstleve, R. W., McCoy, A. J., Moriarty, N. W., Oeffner, R., Read, R. J., Richardson, D. C., Richardson, J. S., Terwilliger, T. C., and Zwart, P. H. (2010) PHENIX: a comprehensive Python-based system for macromolecular structure solution. *Acta Crystallogr. D Biol. Crystallogr.* **66,** 213–221
43. Blanc, E., Roversi, P., Vonrhein, C., Flensburg, C., Lea, S. M., and Bricogne, G. (2004) Refinement of severely incomplete structures with maximum likelihood in BUSTER-TNT. *Acta Crystallogr. D Biol. Crystallogr.* **60,** 2210–2221
44. Emsley, P., Lohkamp, B., Scott, W. G., and Cowtan, K. (2010) Features and development of Coot. *Acta Crystallogr. D Biol. Crystallogr.* **66,** 486–501
45. Chen, V. B., Arendall, W. B., 3rd, Headd, J. J., Keedy, D. A., Immormino, R. M., Kapral, G. J., Murray, L. W., Richardson, J. S., and Richardson, D. C. (2010) MolProbity: all-atom structure validation for macromolecular crystallography. *Acta Crystallogr. D Biol. Crystallogr.* **66,** 12–21
46. Potterton, L., McNicholas, S., Krissinel, E., Gruber, J., Cowtan, K., Emsley, P., Murshudov, G. N., Cohen, S., Perrakis, A., and Noble, M. (2004) Developments in the CCP4 molecular-graphics project. *Acta Crystallogr. D Biol. Crystallogr.* **60,** 2288–2294
47. Burke, J. E., Karbarz, M. J., Deems, R. A., Li, S., Woods, V. L., Jr., and Dennis, E. A. (2008) Interaction of group IA phospholipase A_2 with metal ions and phospholipid vesicles probed with deuterium exchange mass spectrometry. *Biochemistry* **47,** 6451–6459
48. Dole, V. P. (1956) A relation between non-esterified fatty acids in plasma and the metabolism of glucose. *J. Clin. Investig.* **35,** 150–154
49. Plante, M., Bailey, B., and Acworth, I. (2009) The use of charged aerosol detection with HPLC for the measurement of lipids. *Methods Mol. Biol.* **579,** 469–482
50. Batzri, S., and Korn, E. D. (1973) Single bilayer liposomes prepared without sonication. *Biochim. Biophys. Acta* **298,** 1015–1019
51. Kalbfleisch, T., Cambon, A., and Wattenberg, B. W. (2007) A bioinformatics approach to identifying tail-anchored proteins in the human genome. *Traffic* **8,** 1687–1694
52. di Guan, C., Li, P., Riggs, P. D., and Inouye, H. (1988) Vectors that facilitate the expression and purification of foreign peptides in Escherichia coli by fusion to maltose-binding protein. *Gene* **67,** 21–30
53. Ren, X., Lin, J., Jin, C., and Xia, B. (2010) ^{1}H, ^{13}C and ^{15}N resonance assignments of human H-REV107 N-terminal domain. *Biomol. NMR Assign.* **4,** 175–178
54. Evans, P. (2006) Scaling and assessment of data quality. *Acta Crystallogr. D Biol. Crystallogr.* **62,** 72–82
55. Krissinel, E., and Henrick, K. (2004) Secondary-structure matching (SSM), a new tool for fast protein structure alignment in three dimensions. *Acta Crystallogr. D Biol. Crystallogr.* **60,** 2256–2268
56. Collaborative Computational Project, Number 4 (1994) The CCP4 suite: programs for protein crystallography. *Acta Crystallogr. D Biol. Crystallogr.* **50,** 760–763
57. Deems, R. A., Eaton, B. R., and Dennis, E. A. (1975) Kinetic analysis of phospholipase A_2 activity toward mixed micelles and its implications for the study of lipolytic enzymes. *J. Biol. Chem.* **250,** 9013–9020
58. Carman, G. M., Deems, R. A., and Dennis, E. A. (1995) Lipid signaling enzymes and surface dilution kinetics. *J. Biol. Chem.* **270,** 18711–18714
59. Plückthun, A., and Dennis, E. A. (1982) Acyl and phosphoryl migration in lysophospholipids: importance in phospholipid synthesis and phospholipase specificity. *Biochemistry* **21,** 1743–1750
60. Polgár, L. (1974) Mercaptide-imidazolium ion-pair: the reactive nucleophile in papain catalysis. *FEBS Lett.* **47,** 15–18
61. Kamphuis, I. G., Kalk, K. H., Swarte, M. B., and Drenth, J. (1984) Structure of papain refined at 1.65 Å resolution. *J. Mol. Biol.* **179,** 233–256
62. Kortemme, T., and Creighton, T. E. (1995) Ionisation of cysteine residues at the termini of model α-helical peptides. Relevance to unusual thiol pK_a values in proteins of the thioredoxin family. *J. Mol. Biol.* **253,** 799–812
63. van Tienhoven, M., Atkins, J., Li, Y., and Glynn, P. (2002) Human neuropathy target esterase catalyzes hydrolysis of membrane lipids. *J. Biol. Chem.* **277,** 20942–20948
64. Kienesberger, P. C., Lass, A., Preiss-Landl, K., Wolinski, H., Kohlwein, S. D., Zimmermann, R., and Zechner, R. (2008) Identification of an insulin-regulated lysophospholipase with homology to neuropathy target esterase. *J. Biol. Chem.* **283,** 5908–5917
65. Xie, M., Yang, D., Matoney, L., and Yan, B. (2003) Rat NTE-related esterase is a membrane-associated protein, hydrolyzes phenyl valerate, and interacts with diisopropylfluorophosphate through a serine catalytic machinery. *Arch. Biochem. Biophys.* **416,** 137–146
66. Hsu, Y. H., Burke, J. E., Li, S., Woods, V. L., Jr., and Dennis, E. A. (2009) Localizing the membrane binding region of Group VIA Ca^{2+}-independent phospholipase A_2 using peptide amide hydrogen/deuterium exchange mass spectrometry. *J. Biol. Chem.* **284,** 23652–23661
67. Cao, J., Hsu, Y. H., Li, S., Woods, V. L., and Dennis, E. A. (2011) Lipoprotein-associated phospholipase A_2 interacts with phospholipid vesicles via a surface-disposed hydrophobic α-helix. *Biochemistry* **50,** 5314–5321
68. DiSepio, D., Ghosn, C., Eckert, R. L., Deucher, A., Robinson, N., Duvic, M., Chandraratna, R. A., and Nagpal, S. (1998) Identification and characterization of a retinoid-induced class II tumor suppressor/growth regulatory gene. *Proc. Natl. Acad. Sci. U.S.A.* **95,** 14811–14815
69. Moise, A. R., Golczak, M., Imanishi, Y., and Palczewski, K. (2007) Topology and membrane association of lecithin:retinol acyltransferase. *J. Biol. Chem.* **282,** 2081–2090
70. Moise, A. R., Grant, J. R., Lippé, R., Gabathuler, R., and Jefferies, W. A. (2004) The adenovirus E3–6.7K protein adopts diverse membrane topologies following posttranslational translocation. *J. Virol.* **78,** 454–463
71. Xu, Q., Rawlings, N. D., Chiu, H. J., Jaroszewski, L., Klock, H. E., Knuth, M. W., Miller, M. D., Elsliger, M. A., Deacon, A. M., Godzik, A., Lesley, S. A., and Wilson, I. A. (2011) Structural analysis of papain-like NlpC/P60 superfamily enzymes with a circularly permuted topology reveals potential lipid binding sites. *PLoS One* **6,** e22013
72. Tokumura, A., Majima, E., Kariya, Y., Tominaga, K., Kogure, K., Yasuda, K., and Fukuzawa, K. (2002) Identification of human plasma lysophospholipase D, a lysophosphatidic acid-producing enzyme, as autotaxin, a multifunctional phosphodiesterase. *J. Biol. Chem.* **277,** 39436–39442
73. Lord, C. C., Betters, J. L., Ivanova, P. T., Milne, S. B., Myers, D. S., Madenspacher, J., Thomas, G., Chung, S., Liu, M., Davis, M. A., Lee, R. G., Crooke, R. M., Graham, M. J., Parks, J. S., Brasaemle, D. L., Fessler, M. B., Brown, H. A., and Brown, J. M. (2012) CGI-58/ABHD5-derived signaling lipids regulate systemic inflammation and insulin action. *Diabetes* **61,** 355–363
74. Montero-Moran, G., Caviglia, J. M., McMahon, D., Rothenberg, A., Subramanian, V., Xu, Z., Lara-Gonzalez, S., Storch, J., Carman, G. M., and Brasaemle, D. L. (2010) CGI-58/ABHD5 is a coenzyme A-dependent lysophosphatidic acid acyltransferase. *J. Lipid Res.* **51,** 709–719
75. Kumari, M., Schoiswohl, G., Chitraju, C., Paar, M., Cornaciu, I., Rangrez, A. Y., Wongsiriroj, N., Nagy, H. M., Ivanova, P. T., Scott, S. A., Knittelfelder, O., Rechberger, G. N., Birner-Gruenberger, R., Eder, S., Brown, H. A., Haemmerle, G., Oberer, M., Lass, A., Kershaw, E. E., Zimmermann,

R., and Zechner, R. (2012) Adiponutrin functions as a nutritionally regulated lysophosphatidic acid acyltransferase. *Cell Metab.* **15,** 691–702
76. Ferry, G., Tellier, E., Try, A., Grés, S., Naime, I., Simon, M. F., Rodriguez, M., Boucher, J., Tack, I., Gesta, S., Chomarat, P., Dieu, M., Raes, M., Galizzi, J. P., Valet, P., Boutin, J. A., and Saulnier-Blache, J. S. (2003) Autotaxin is released from adipocytes, catalyzes lysophosphatidic acid synthesis, and activates preadipocyte proliferation. Up-regulated expression with adipocyte differentiation and obesity. *J. Biol. Chem.* **278,** 18162–18169
77. Lass, A., Zimmermann, R., Haemmerle, G., Riederer, M., Schoiswohl, G., Schweiger, M., Kienesberger, P., Strauss, J. G., Gorkiewicz, G., and Zechner, R. (2006) Adipose triglyceride lipase-mediated lipolysis of cellular fat stores is activated by CGI-58 and defective in Chanarin-Dorfman syndrome. *Cell Metab.* **3,** 309–319
78. Subramanian, V., Rothenberg, A., Gomez, C., Cohen, A. W., Garcia, A., Bhattacharyya, S., Shapiro, L., Dolios, G., Wang, R., Lisanti, M. P., and Brasaemle, D. L. (2004) Perilipin A mediates the reversible binding of CGI-58 to lipid droplets in 3T3-L1 adipocytes. *J. Biol. Chem.* **279,** 42062–42071
79. Baulande, S., Lasnier, F., Lucas, M., and Pairault, J. (2001) Adiponutrin, a transmembrane protein corresponding to a novel dietary- and obesity-linked mRNA specifically expressed in the adipose lineage. *J. Biol. Chem.* **276,** 33336–33344
80. Brown, J. M., Betters, J. L., Lord, C., Ma, Y., Han, X., Yang, K., Alger, H. M., Melchior, J., Sawyer, J., Shah, R., Wilson, M. D., Liu, X., Graham, M. J., Lee, R., Crooke, R., Shulman, G. I., Xue, B., Shi, H., and Yu, L. (2010) CGI-58 knockdown in mice causes hepatic steatosis but prevents diet-induced obesity and glucose intolerance. *J. Lipid Res.* **51,** 3306–3315
81. Chanarin, I., Patel, A., Slavin, G., Wills, E. J., Andrews, T. M., and Stewart, G. (1975) Neutral-lipid storage disease: a new disorder of lipid metabolism. *Br. Med. J.* **1,** 553–555
82. Dorfman, M. L., Hershko, C., Eisenberg, S., and Sagher, F. (1974) Ichthyosiform dermatosis with systemic lipidosis. *Arch. Dermatol.* **110,** 261–266
83. Lefèvre, C., Jobard, F., Caux, F., Bouadjar, B., Karaduman, A., Heilig, R., Lakhdar, H., Wollenberg, A., Verret, J. L., Weissenbach, J., Ozgüc, M., Lathrop, M., Prud'homme, J. F., and Fischer, J. (2001) Mutations in CGI-58, the gene encoding a new protein of the esterase/lipase/thioesterase subfamily, in Chanarin-Dorfman syndrome. *Am. J. Hum. Genet.* **69,** 1002–1012
84. Federico, L., Ren, H., Mueller, P. A., Wu, T., Liu, S., Popovic, J., Blalock, E. M., Sunkara, M., Ovaa, H., Albers, H. M., Mills, G. B., Morris, A. J., and Smyth, S. S. (2012) Autotaxin and its product lysophosphatidic acid suppress brown adipose differentiation and promote diet-induced obesity in mice. *Mol. Endocrinol.* **26,** 786–797
85. Dusaulcy, R., Daviaud, D., Pradère, J. P., Grès, S., Valet, P., and Saulnier-Blache, J. S. (2009) Altered food consumption in mice lacking lysophosphatidic acid receptor-1. *J. Physiol. Biochem.* **65,** 345–350
86. Ahmadian, M., Duncan, R. E., Varady, K. A., Frasson, D., Hellerstein, M. K., Birkenfeld, A. L., Samuel, V. T., Shulman, G. I., Wang, Y., Kang, C., and Sul, H. S. (2009) Adipose overexpression of desnutrin promotes fatty acid use and attenuates diet-induced obesity. *Diabetes* **58,** 855–866
87. Diederichs, K., and Karplus, P. A. (1997) Improved R-factors for diffraction data analysis in macromolecular crystallography. *Nat. Struct. Biol.* **4,** 269–275
88. Weiss, M. S. (2001) Global indicators of x-ray data quality. *J. Appl. Crystallogr.* **34,** 130–135